# Detection of Globotriaosylceramide (Gb3) in a HEK cell model

**Teresa da Cunha e Silva Lopes Santos**

Thesis to obtain the Master of Science Degree in

**Biological Engineering**

Supervisors:

Dr. Osvaldo Daniel Uchitel

Prof. Cláudia Alexandra Martins Lobato da Silva

## Examination Committee

Chairperson: Prof. Gabriel António Amaro Monteiro

Supervisor: Dr. Osvaldo Daniel Uchitel

Member of the Committee: Prof. Ana Maria Ferreira de Sousa Sebastião

**March 2023**

## Preface

The work presented in this thesis was performed at IFIBYNE – Institute of Physiology, Molecular Biology and Neurosciences (Buenos Aires, Argentina), between April 2022 and November 2022, under the supervision of Dr. Osvaldo Uchitel. The thesis was co-supervised at Instituto Superior Técnico by Professor Cláudia Lobato da Silva.

I declare that this document is an original work of my own authorship and that it fulfils all the requirements of the Code of Conduct and Good Practices of the Universidade de Lisboa.

To my family: who always gave me the wings to fly to my dreams, who always gave me the support in the greatest adversities that life offers us, who always gave me, and still gives me, the strength to live.

# Acknowledgments

First of all, I must thank Dr.Osvaldo Uchitel for accepting me in his project, for welcoming me with open arms, for his friendliness and constant availability. To Professor Cláudia Lobato, who, even with all the distance that separated us, was always a constant support, a friendly and reassuring word - I am eternally grateful to her for having helped me in this huge challenge in my life.

To Carina Weissman, who, although with no official title, was a spectacular advisor. I praise her for her patience with me and her dedication to teaching. A huge thank you for all the help in the work developed, it wouldn't be possible without you. I also take this opportunity to thank Catarina Castellanos, Georgina Mingolo and Mayra Montes, for all the fantastic work they always did, and for all the snacks they always provided.

A heartfelt thank you to Natalia Gobetto, who was the work partner and friend I needed to get me through my day to day. Her fun personality, her charisma and her good humour made all the work easier. I carry her in my heart and hope that we will meet again, and perhaps work together.

To my oldest friends, Constança, Inês, Rita, Filipa, Maria, Francisco, Miguel, Bernardo, Afonso, Diogo and Rodrigo, my true and faithful ones, who, although far away, have always accompanied me in this stage, with a presence and importance that not even they know; and also to my new friends, from the 4 corners of the world, who have taught me the pleasure of meeting new cultures and have been the essential support and company for an exchange experience.

There are not enough words to describe what I must thank my family and dogs for. I understood the meaning of the expression "*You only appreciate them when you lose them*"; not that I lost them, I know they are the most solid thing in my life but being away from them for so long only made me realise how important they are to me, the unconditional and infinite love I feel for them, the true meaning of the word *"Saudade".* To my sister, who gave me the happiness to become an aunt, to feel a distinct love, to know what it is to take care of a being, and for, also a thank you to my nephew, who, even without being born yet, is already my guardian angel.

Finally, I leave my thanks to those who made my heart Argentine, who taught me what it is to give oneself, what it is to share, to live together and what it is to love someone. I thank my boyfriend, Pedro, for holding my hand every day, at every moment and for making me fight and conquer my happiness. I know that without him it wouldn't be possible, and that's why I leave my heart in Argentina.

# Abstract

Fabry disease is a rare disorder within the spectrum of progressive lysosomal overload diseases. It is characterised by the deficient or absent lysosomal activity of α-galactosidase A, which results in the accumulation of globotriaosylceramide (Gb3). The accumulation of this glycosphingolipid causes some of the typical symptoms of Fabry's disease, as the appearance of angiokeratomas and neuropathic pain.

In this project, the detection of Gb3 was studied using a model of HEK cells treated with drugs that produce the accumulation of Gb3 to then determine the optimal parameters that allow detection by microscopy. To determine the incubation time at which the intensity levels were higher, that is, there was a greater accumulation of Gb3, two different times were studied, a 30-minute incubation time and a 2-hour incubation time. The results obtained for Gb3, Lyso-Gb3 and DGJ were also compared with each other.

Increased Gb3 incorporation was observed in the treated cells, as well as increased accumulation in the plasma membrane, with higher values obtained for the two-hour incubation. Given its functional diversity, it would be interesting to continue studying the detection and location of Gb3, to contribute to the development of new and more effective therapies. Once it has been determined how and where this glycolipid accumulates, it would be beneficial to study how it is eliminated from the organ, its metabolization and degradation.



**Keywords:** Fabry’s disease, Globotriaosylceramide, Glycosphingolipid, Angiokeratomas, Neuropathic pain, Lyso-Gb3, 1-Deoxygalactonojirimycin

# Resumo

A doença de Fabry é uma doença rara do espetro das doenças de sobrecarga lisossomal progressiva. É caracterizada por uma atividade lisossomal deficiente, ou ausente, da enzima alfa-galactosidase A, resultando na acumulação de globotriaosilceramida (Gb3). A acumulação deste glicolípido é o responsável pelos sintomas característicos da doença de Fabry, como o aparecimento de angioqueratomas e dor neuropática.

Neste projeto estudou-se a deteção de Gb3, recorrendo a um modelo de células HEK tratadas com compostos que produzem a acumulação de Gb3 para logo determinar os parâmetros ótimos que permitem a deteção por microscopia de fluorescência. De modo a perceber qual o tempo de incubação onde a intensidade de fluorescência era maior, ou seja, a acumulação de Gb3 era superior, foram analisados os resultados para dois tempos distintos, 30 minutos e 2 horas. Foram também comparados entre si os resultados obtidos para Gb3, Lyso-Gb3 e DGJ.

Verificou-se um aumento da incorporação de Gb3 nas células sujeitas a tratamento, bem como um aumento da acumulação do mesmo na membrana plasmática, com valores superiores para o tempo de incubação de duas horas. Dada a sua diversidade funcional, seria interessante continuar com o estudo da deteção e localização do Gb3, contribuindo para o desenvolvimento de novas e mais eficazes terapias. Já determinado onde e como se acumula este glicolípido, seria benéfico estudar como é eliminado do órgão, a sua metabolização e degradação.



**Palavras-chave:** Doença de Fabry, Globotriaosilceramida, Glicoesfingolípido, Angioqueratomas, Dor neuropática, Lyso-Gb3, 1-Desoxigalactonojirimicn

# Contents

# List of Tables

# List of Figures

## List of Abbreviations

**FD** Fabry Disease

**ASIC** Acid-sensing ion channel

**GSL** Glycosphingolipid

**Gb3** Globotriaosylceramide

**Lyso-Gb3** Globotriaosylsphingosine

**SF** Small Fibers

**ERT** Enzyme replacement therapy

**PCR** Polymerase Chain Reaction

**PLL** Poly-L-Lysine

**Rv** Reverse

**Fw** Forward

**FC** *Fabry Control*

**FM** *Fabry Mutant*

**FW** *Fabry Wild-Type*

**WT** *Wild-Type*

**KO** *Knockout*

**ROI** region of interest

**$IC_{50}$** Half-maximal inhibitory concentration

# 1 Introduction

## 1.1 Fabry Disease

### 1.1.1 Overview

Fabry disease (FD) is a rare disease, with a prevalence estimated to be between 1:40 000 and 170 000, however, these values may underestimate the true prevalence of the disease.[1] The rarity of the disease may be attributable to its sex-linked mode of transmission.

Affected males transmit the genetic mutation only to female offspring, producing females heterozygous for Fabry disease. FD is now considered to be a broad-spectrum disease, revealing heterogeneous and progressive phenotypes, more severe in men, and asymptomatic in women [2] Some of the most frequent symptoms, as well as the first to appear, include chronic neuropathic pain and episodic severe pain crises.

Fabry disease (FD) belongs to the group of lysosomal storage disorders, that is, inborn errors of metabolism characterized by the accumulation of undegraded macromolecules in lysosomes due to a deficiency of one of the lysosomal enzymes. This disease is caused by pathogenic mutations in the α-galactosidase A (GLA) gene, located on X chromosome (Xq22.1).[3] There are distinct and different mutations that can occur in the GLA gene and cause Fabry disease, such as missense, nonsense, consensus splice site, cryptic splicing and frameshift mutations. So far, more than 400 mutations have been recorded in the α-Gal A gene GLA; these mutations, caused mostly by single amino acid substitutions, lead to its early degradation within the endoplasmic reticulum and prohibit intracellular trafficking of the enzyme to the lysosome, as a consequence of this mutation, there is an accumulation of substrates globotriaosylceramide (Gb3) and globotriaosylsphingosine (Lyso-Gb3) in a variety of cell types, including capillary endothelial cells, renal (podocytes, tubular cells, glomerular endothelial, mesangial and interstitial cells), cardiac (cardiomyocytes and fibroblasts) and nerve cells.[4]

Figure 1.1a) represents the catabolism of macromolecules by the enzyme α-galactosidase, catalysing the removal of galactose from oligosaccharides, glycoproteins, and glycolipids. Figure 1.1b) represents the lack of enzyme α-galactosidase that causes the accumulation of globotriaosylceramide in the tissues, characteristic of Fabry disease.[5]

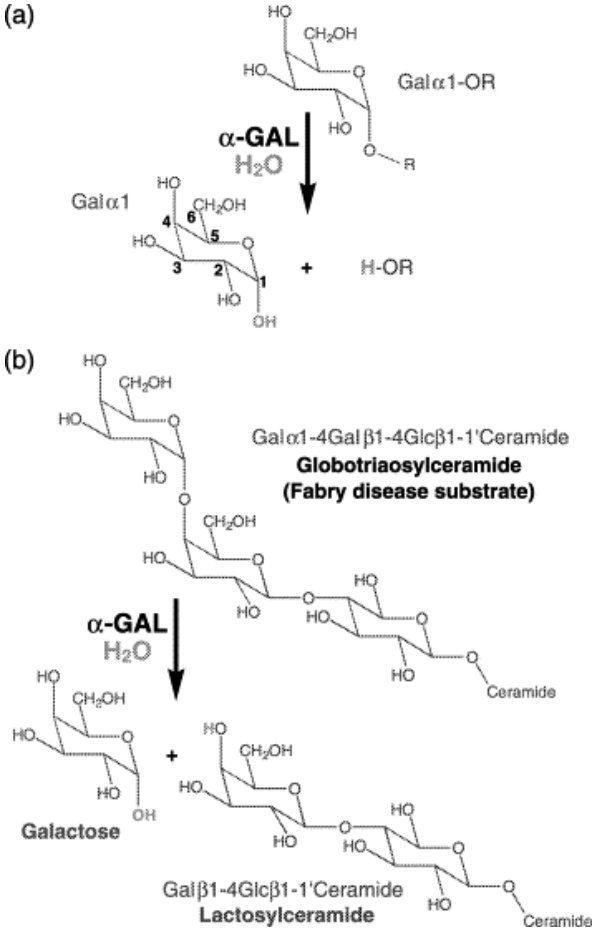


**Figure 1.1** - Catabolism of macromolecules made by α-Gal A enzyme, responsible for removing galactose from oligosaccharides, glycoproteins, and glycolipids (Figure 1.1a). The absence of an enzyme causes the accumulation of galactosylated substrates (primarily globotriaosylceramide) in the tissues, typical of Fabry disease (Figure 1.1b).[6]

The α-Gal A enzyme is a homodimeric glycoprotein with each monomer composed of two domains; a $(\beta/\alpha)_8$, containing the active site, and a C-terminal domain containing eight antiparallel β strands on two sheets in a β sandwich. The structure of α-Gal A monomer, with its respective domains, is represented in Figure 1.2.[6]

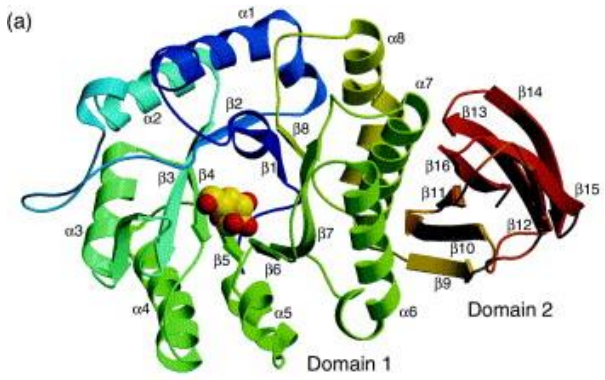


**Figure 1.2** - Structure of α-Gal A enzyme, with identification of the respective domains.[6]

In Figure 1.3 are represented the location of Fabry disease mutations.

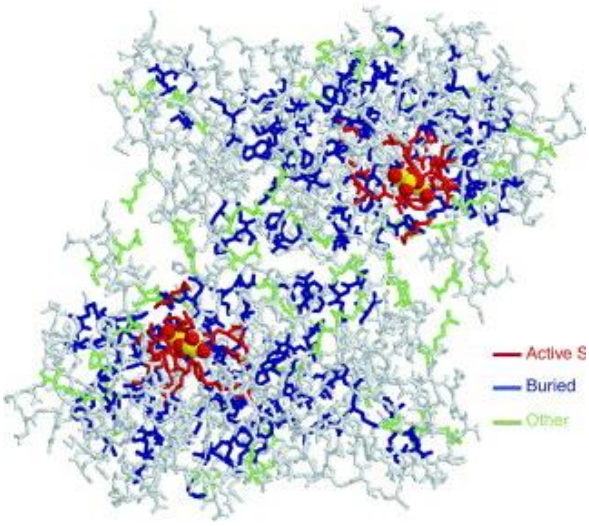


**Figure 1.3** – α-Gal A enzyme mutations characteristic of Fabry disease.[6]

Mutations characterised by reduced or no α-Gal A activity are responsible for the most severe phenotype, known as classic Fabry disease.[7]

The prevalence and severity of Fabry disease have led to the need for the development of therapies to alleviate its characteristic symptoms. The most widely used therapy with the most favourable results is Enzyme Replacement Therapy (ERT). This therapy introduces recombinant enzyme α–Gal A into lysosomes to help address the underlying enzyme deficiency and restore the breakdown of accumulated Gb3 in patients with Fabry disease, in addition to the associated multisystemic disease manifestations.

### 1.1.2 Globotriaosylceramide (Gb3)

The glycosphingolipid (GSL) is a complex group of lipids involved in distinct cellular events that include the regulation of membrane-receptor protein signalling, cellular crosstalk, cell adhesion and differentiation. The globotriaosylceramide (Gb3) is a glycosphingolipid formed by a lipid skeleton connected to an oligosaccharide.[8] Figure 1.4 shows the structure of Gb3 depicting the lipid part attached to sphingosine and a fatty acid via an amide bond.

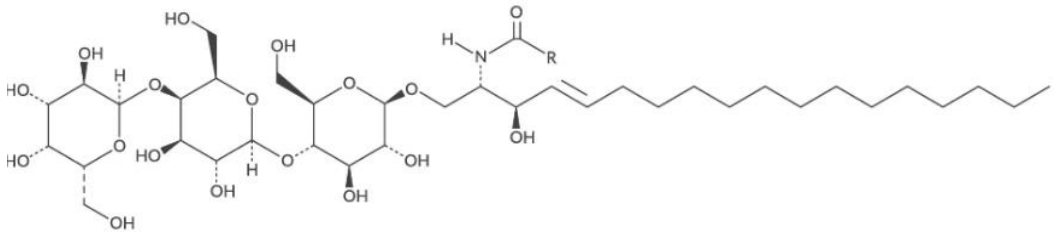

**Figure 1.4** – Structure of globotriasosylceramide, with the lipid part attached to a sphingosine and a fatty acid by an amide bond.[9]

Gb3 molecules can be modified to so-called analogues or isoforms, if the modification is in the sphingosine or the fatty acid chain, respectively. Although the location of Gb3 varies from species to species, it is often identified in the outer layer of the cell membrane of many different cell types and is part of lipid rafts.[8]

In Fabry Disease, this glycosphingolipid progressively accumulates in lysosomes and other cellular compartments and can therefore be considered a disease-specific marker. The microvascular endothelial accumulation of this glycolipid causes the appearance of angiokeratomas, while its accumulation in the podocytes of several renal cells is responsible for a decrease in glomerular filtration with subsequent renal failure.[10]

However, there may be other components besides Gb3, such as globotriaosylsphingosine (Lyso-Gb3), a deacylated form of Gb3. Lyso-Gb3 has been proposed to play a causative role in Fabry disease pathogenesis by accelerating Gb3 storage and may also be involved in pain. Figure 1.5 depicts the chemical structure of Lyso-Gb3.

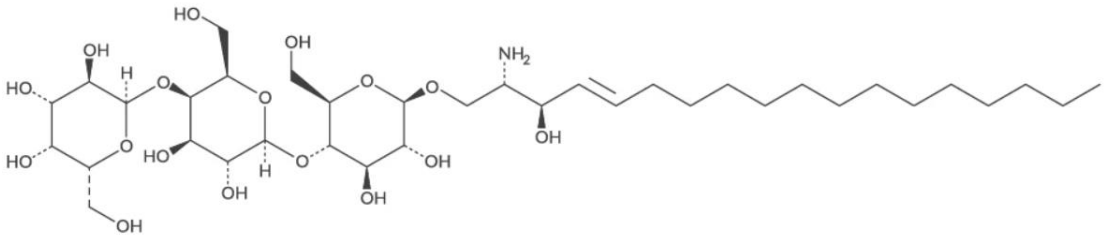

**Figure 1.5** – Structure of globotriaosylsphingosine, with its lipid part connected to a sphingosine and a fatty acid by an amide bond.[9]

Recently, several studies have revealed the potential of Lyso-Gb3 as a biomarker for Fabry disease since it is water-soluble and circulates in concentrations 300-500 times higher than normal. Although Lyso-Gb3 has been described as a biomarker capable of reflecting disease severity and therapeutic monitoring, it exhibits several toxic effects as a metabolite, as it promotes Notch1-mediated inflammation and disrupts the gut microbiota homeostasis modulating the biofilm formation, triggering the typical gastrointestinal symptoms of Fabry disease. [11]

Some hypotheses try to relate the presence of Gb3 to the development of pain. One of them concludes that accumulation of Gb3 in DRG neurons can reduce intraepidermal nerve fibre density and interfere with the function of cellular membrane proteins, promoting cytotoxicity and resulting in nerve fibre dysfunction.[12]

A second hypothesis concerns chronic nerve ischemia secondary to Gb3 deposition within the endothelial cells of the blood vessels supplying nerve fibres.[13]

## 1.2 ASICs channels

ASICs, also called proton-gated channels, belong to the epithelial sodium channel/DeGenerin superfamily and can be voltage-independent, amiloride-sensitive, cation-selective, and particularly sensitive to protons.[5,14]

These channels display 7 distinct subunits (ASIC1a, ASIC1b1, ASIC1b2, ASIC2a, ASIC2b, ASIC3 and ASIC4), encoded by four genes and expressed mainly in the nervous system. ASIC1a, a key subunit in the central nervous system, shows, in addition to its $Na^+$ permeability, a small permeability to $Ca^{2+}$. The importance of ASIC1a in the CNS is underlined by the fact that it is involved in several neurodegenerative diseases and plays a prominent role in neuronal death.[5,15]

Figure 1.6 represents the structure of ASICs channels, with their hydrophobic transmembrane regions, acidic pocket, N and C terminals and the extracellular domain.[16]

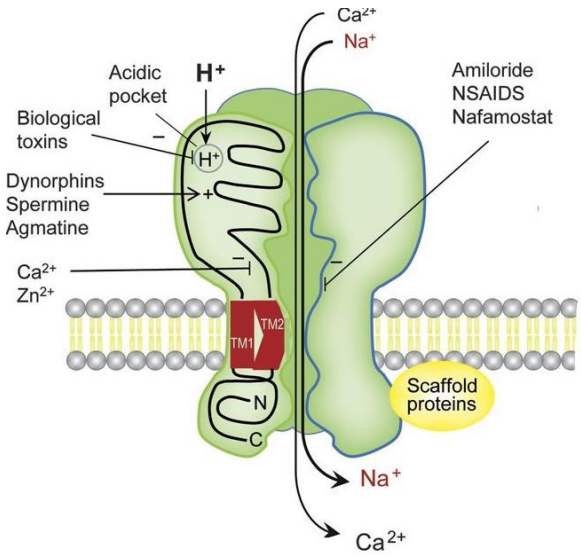


**Figure 1.6** – General structure of ASICs, with the respective hydrophobic domains, acidic pocket, amino and carboxy terminals and the extracellular domain.[16]

ASIC channels, particularly ASIC1a, are upregulated in Fabry disease as a result of glycosphingolipid accumulation.[17] The relationship between intracellular deposits of Gb3 and dysfunctions in neuronal ion channels has already been demonstrated since it causes consequences in the interaction of the extra lysosomal lipid with the raft or an effect on protein mRNA regulation.[18] It was also found an upregulation of these same channels in inflammatory pain hypersensitivity, one of the most severe symptoms of Fabry disease.[19]

## 1.3 Preclinical models of Fabry disease

To understand the pathophysiology and some symptoms of Fabry disease, different models have been developed, such as *in vitro* cell cultures and preclinical animal models.

There are different *in vitro* models to study Fabry disease, such as mammalian expression systems, human cell lines, insect cells, induced pluripotent stem cells (iPSCs), tobacco cells, and many different ones that are still under study.

These models have been increasingly used because of their advantages and the contribution they make to the discovery of promising drug targets that can be tested in future clinical trials. Some of the major advantages presented by this type of model are the possibility to have a fine-tuned and precise control of the physicochemical properties of the environment as well as the physiological conditions, a reduction in the duration and costs of translation to clinical trials by helping to identify the mechanism of action, higher throughput, and the opportunity to reduce the use of animal models. The disadvantage that arises from this method is that they fail to replicate the conditions of cells in an organism.[20,21]

Animal models and *in vivo* studies are also very useful to study the symptoms of Fabry disease, especially pain. This type of model has several advantages since it can mimic the biological process or disease found in humans, given the notorious physiological and anatomical similarities that exist between humans and animals. Despite these advantages, the use of animal models has many ethical issues associated with them, as there is debate about how sensible it is to use animals to benefit human purposes, with the possibility that animals are harmed.

### 1.3.1 HEK cell line

The HEK cell line has been increasingly used as an *in vitro* cell culture system and as an expression tool for recombinant proteins given its high transfection efficiency and capacity to carry out most of the post-translation folding and processing required to generate functional and mature proteins.[22]

HEK298, also often referred to as HEK cells, corresponds to an immortal cell line derived from human embryonic kidney cells grown in tissue culture. This particular cell line was initiated by the transformation and culturing of normal HEK cells with sheared fragments of human adenovirus type 5 (Ad5) DNA.

The easy and fast reproduction, high efficiency of transfection and protein production, ease of growth in suspension serum-free culture, consistency in the results obtained and highly reproducible, make HEK cell one of the best options for cell model studies. However, they are more sensitive to viral or bacterial contamination. Another limitation is the culture period. Even for immortalized cell lines, culturing for extended periods will cause the health of cells to degrade. This affects the growth rate and translation efficiency of the cells.[23]

These cells can be sourced from American Type Culture Collection (ATCC: Manassas, USA) under the designation “293”. Although culturing these cells is not complicated or highly maintained, there are specific HEK cell line requirements that must be maintained to ensure cell growth and viability.

HEK cells are usually cultured as an adherent monolayer and can be continuously cultured at 37ºC in a 5% $CO_2$:95% air humidified incubator, in a high-glucose media.

The confluence of the cell culture is vital to the cell splitting process and is determined by how much of the plate is covered in cells. HEK cells remain biochemically active at 50-70% confluency and are enzymatically harvested when reaching 70% confluence. Is easy to see when cells die as their size is significantly smaller and they are darker than living cells. One other quick way to monitor cell health is by the colour of the media. The media (DMEM) will begin to turn orange and yellow as more dead cells collect in the media, causing the media to become more basic.[23]

HEK 293 cells are used in an extensive range of research applications. One major application for HEK293 and its derived cell lines lies in fundamental research, as it allows for the detailed investigation of human proteins in a cellular background. Another widespread use for HEK293-derived cell lines is the heterologous expression of ion channels and cell membrane receptors. HEK cells are also used to produce viral particles such as lentiviral particles that, in turn, can for instance be used to transduce non-dividing cells.[22]

### 1.3.2 Animal Models

As previously mentioned, the use of animal models brings many advantages to the study of the physiology and symptoms of certain diseases, given all the anatomical similarities between humans and animals.

The most used model is the rodent, and Fabry models are obtained in different forms. The α-Gal A-knockout (GLAko) mouse has been used as a model of Fabry disease and was generated by targeted disruption of the murine α-Gal A gene (GLA).[24] This model accumulates Gb3 in the kidney and liver, but only 25% of what is found in Fabry disease patients, thus failing to mimic the typical Fabry disease phenotype.[25]

The genetic background of Fabry mice that originated from the National Institutes of Health was a mixture of C57BL/6 (B6) and 129 strains. The first generation of heterozygous female mice was the result of crossing Fabry-B6/129 hemizygous male mice and WT B6:129S F1 hybrid females, from Jackson Laboratory. Figure 1.7 represents the crossbreeding that led to the creation of the Fabry colony used to replicate this disease.

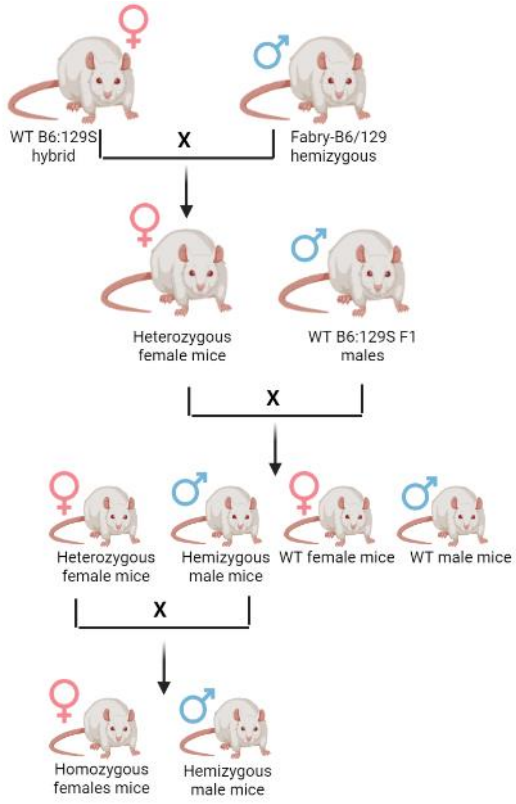


**Figure 1.7** - Steps in the process of crossing between different mouse species to create the Fabry colony. Fabry-B6/129 hemizygous male mice were crossed with WT B6:129S F1 hybrid females (Jackson Laboratory) to generate heterozygous female mice. These heterozygotes were crossed with WT B6:129S F1 males (Jackson Laboratory) to generate heterozygous females, hemizygous males, and WT males and females. Homozygous females and hemizygous males were generated by crossing the above heterozygotes and hemizygotes, from which a Fabry colony was generated.

Validation and confirmation of the animal model genotype are done by PCR technique. This technique presents advantages such as high sensitivity, including the elimination of post-amplification handling and processing of large numbers of samples. However, its high complexity and sensitivity makes this method very susceptible to contamination.[26]

# 2 Goal of the Project

The present study was conducted in the IFIBYNE Laboratory – Institute of Physiology, Molecular Biology and Neurosciences of the Faculty of Exact Sciences of the University of Buenos Aires, from April to November 2022. The main goal is to detect Gb3 and Lyso-Gb3 by immunohistochemistry in HEK cell model for subsequent detection in animal tissues of the Fabry disease model. For this, HEK cells will be cultured with drugs that produce an intracellular accumulation of Gb3, such as DGJ, an inhibitor of the enzyme whose substrate is Gb3, to determine the optimal parameters that allow detection by fluorescence microscopy.

Globotriaosylceramide (Gb3) is a glycosphingolipid that accumulates progressively, mainly in lysosomes and other cellular compartments in Fabry disease. Dr.Osvaldo Uchitel's working group had previously evaluated the incorporation of Gb3 into HEK cells from Gb3 tagged with a fluorescent probe; however, work remains to be done to understand the correlation between this glycosphingolipid and Fabry disease.

In parallel to the work with HEK cells, and to validate the genotype of Fabry model mice, either WT or GLA KO, amplification of the respective DNA segments by PCR was performed and an electrophoresis gel was to run the respective samples. Fabry model mice are created by the α-Galactosidase A gene knockout (GLA KO), which invalidates the enzyme activity and causes Gb3 to accumulate in tissues, mimicking what happens in Fabry disease.

# 3 Materials and Methods

## 3.1 Cellular and molecular biology

This study was performed with the HEK cell line, derived from human embryonic kidney cells. HEK cells present were obtained from American Type Culture Collection (ATCC, Manassas, USA). HEK cells were grown in Dulbecco's Modified Eagle's Medium containing 4 mM L-glutamine, 4.5 g/L glucose, and 110 mL/L sodium pyruvate and supplemented with 10% Fetal Calf Serum (NatoCor).

The cells were kept under humidified atmosphere, at 37ºC and 5% CO to grow in monolayers in 6 multiwell plates. The medium was changed twice a week or when the cells reached 80-90% confluence. HEK cells were maintained by serial passages.

For biochemical and molecular analysis, 6 coverslips were coated with 0.1 mg/mL of poly-L-lysine (PLL) and dissociated HEK cells were plated at a density of 2 x $10^4$ cells. When required to determine the number of viable cells in a certain suspension, cells were counted using a Neubauer chamber.

## 3.2 Immunohistochemistry

### 3.2.1 Materials

The materials and solutions used in immunohistochemistry are represented in Table 3.1 with their respective details.

**Table 3.1** - Different materials and solutions used in immunohistochemistry with respective details.

| Materials and Solutions | Details | Brand |
|---|---|---|
| PLL | 1mg/mL<br>0.1mg/mL in borate buffer | Sigma-Aldrich |
| Wash buffer | 0.1% BSA in PBS<br>0.05% Tx-100 | Sigma-Aldrich<br>Innovative Research |
| Blocking buffer | 5%Serum<br>2%BSA<br>0.1%Triton X-100 in PBS | Sigma-Aldrich<br>Innovative Research |
| PFA 4% in PBS | Aliquots at -20ºC, cell culture | - |
| Permeabilization buffer | 0.1% Tx-100 | Sigma-Aldrich |
| PBS | Dilute from 10x 4C in cell culture, to pH 7.4 | - |
| Glycine | 0.1M | Sigma-Aldrich |

The antibodies, Anti-Gb3 (TCI, TCIAA2586) and Anti-mousse 488 (ThermoFisher, #A-11001), primary and secondary, respectively, as well as other reagents (RNAse and Propidium Iodide), were used in sufficient quantities to cover the coverslip (between 40-50µL). The concentration used of Gb3, Lyso-Gb3 and DGJ was 20µM, 0.4µM and 200µM, respectively.

### 3.2.2 Drugs and Treatments

Three treatments were carried out, each with a different drug (Gb3, Lyso-Gb3 and DGJ). The methodology performed is the same, varying only in the amounts and the incubation time.

Cells in PLL-coated coverslips (3 glasses of density $2x10^4$) were washed and renewed with 400µL of medium.

In each of the experiments, one coverslip was treated either with 1µL of Gb3 (20µM), with 1µL of Lyso-Gb3 (0.4µM), or with 8µL of DGJ (200µM), all in 400µl of DMEM, while another coverslip was treated with 1µl of DMSO in 400µl of DMEM (control to Gb3, Lyso-Gb3 and DGJ treatment). The third coverslip served as a negative control and was treated with 400µl of DMEM and without Anti-Gb3. Subsequently, the whole plate was kept in the incubator at 37ºC for 30 minutes or 2 hours, depending on the treatment performed.

After this time, the medium was washed with PBS. Each of the 3 coverslips was fixated with paraformaldehyde (PFA) 4% for 15 minutes at room temperature (RT). It was followed by a washing step, one time with PBS. After that, 0.1M glycine was added for 15 minutes at RT and permeabilization with Triton X-100 0.1% in PBS was incubated for 5 minutes. Then cells were washed with PBS two times for 2 minutes each and blocked for 45 minutes in blocking buffer followed by overnight incubation with primary antibody Anti-Gb3 Monoclonal Antibody, diluted in blocking buffer. The dilutions performed on this antibody were 1:100 and 1:200.

After further washing steps (5 x 2 minutes) with wash buffer, cells were incubated for 45 minutes at RT with 40µL secondary antibody Anti-mouse 488 (1:500). New wash steps were performed with wash buffer (5 x 2 minutes) for subsequent incubation with RNAse at 37ºC for 20 minutes. The cells were then washed with PBS (2 x 2 minutes) and then treated with propidium iodide (PI) for 5 minutes. A final washing step with PBS (4 x 2 minutes) is performed to finish with the mounting of the coverslips with 3µL mounting medium.

## 3.3 Microscopy

Images were taken using two different microscopes – Confocal FV1000 and Confocal LSM900 microscopes, both with 40x oil-immersion objective. Alexa-488-conjugated secondary antibody as well as PI were excited using an Argon (lambda: 488nm) and Helium-Neon (lambda:543 nm) lasers and a transmission light detector.

## 3.4 Data analysis and presentation

The obtained data were analysed using Student's t-test, ANOVA and Dunnet post hoc tests and plotted using the *GraphPad Prism 8* (GraphPad Software Inc., La Jolla, San Jose, Ca, USA). The statistical analysis performed starts with the evaluation of the normality of the data via a "D'Agostino-Pearson" test and "Shapiro-Wilk" test recommended by the software for this sort of verification.

For analysis of integrated density, images were imported into ImageJ software (NIH) by *Fiji*. To compare the intensity levels between the controls and their treatments, the outline of the cells was manually drawn to obtain ROIs with integrated density for the Gb3, DGJ or Lyso-Gb3 channel. Cell intensity was measured according to the laboratory protocol available at *The Open Lab Book*.[27] Other cell parameters were analysed, such as size and area. The resulting images have undergone some corrections. Background subtraction was used to reduce background noise as much as possible.

## 3.5 Molecular Biology procedures

### 3.5.1 DNA Extraction

DNA samples were extracted from the ears of the mice. To perform the DNA extraction and precipitation, it is necessary to prepare two different solutions. The Alkaline Lysis Reagent, or solution 1, is composed of 20mM NaOH and 0.2mM EDTA. The Neutralization Buffer, or solution 2, is composed of 40mM Tris-HCl.

For DNA extraction, 100µL of solution 1 was added to each ear and then heated to 98ºC for 30 minutes in a thermoblock. Subsequently, 100µL of solution 2 was added and stored in the freezer.

### 3.5.2 Polymerase Chain Reaction

To further validate the genotype of Fabry model mice, an amplification and gel electrophoresis of Polymerase Chain Reaction (PCR) amplification products was performed. The PCR analysis was performed based on the InBio Highway Polymerase Chain Reaction.

There are three distinct primers for amplifying DNA, one of which is common to WT (FC *fw – forward primer*), one specific to WT and one to mutant, both reverse primers (FW *rv* and FM *rv*, respectively). The characteristics of these primers are shown in Table 3.2. The melting temperatures were calculated with the Melting Temperature Calculator from Thermo Fisher Scientific, using a concentration of primer of 0.5µM and considering the usage of the DreamTaq polymerase mixture.

**Table 3.2** - Primers' sequences and melting temperature.

| Primer | Sequence | Melting Temperature (ºC) |
|---|---|---|
| FC *fw* | 5' AGG TCC ACA GCA AAG GAT TG 3' | 59.8 |
| FW *rv* | 3' GCA AGT TGC CCT CTG ACT TC 5' | 60.6 |
| FM *rv* | 3' GCC AGA GGC CAC TTG TGT AG 5' | 62.3 |

**Table 3.3 -** Fragment sizes obtained by PCR of DNA from KO species and WT species.

| | Fragment Size (bp) |
|---|---|
| *Wild Type* | 295 |
| *Gla* KO | 202 |

To perform the PCR technique, it was necessary to prepare the reagents for the MasterMix. Table 3.4 shows these same reagents, making up a total volume of 19µL, to which 6µL of DNA were then added, making a final volume of 25µL.

**Table 3.4 -** Reaction mixture for PCR with DreamTaq DNA polymerase.

| Component | Volume (µL) |
|---|---|
| $Mg^{2+}$(InBio Highway) | 2.09 |
| Buffer (InBio Highway) | 2.38 |
| $H_2O$ Calidad qPCR | 11.5 |
| PrimerFw (MERCK) | 0.95 |
| PrimerRv (MERCK) | 0.48 |
| PrimerFc (MERCK) | 0.48 |
| dNTPs (InBio Highway) | 0.95 |
| DreamTaq DNA polymerase (IFIBYNE Institute) | 0.19 |

The protocol conditions for performing PCR with Taq DNA Polymerase are described in Table 3.5.

**Table 3.5 -** Protocol for PCR with DreamTaq DNA polymerase.

| Step | Temperature (ºC) | Duration | |
|---|---|---|---|
| Initial denaturation | 94 | 2 min | |
| Denaturation | 94 | 45 s | 30 cycles |
| Annealing | 63 | 45 s | |
| Elongation | 72 | 60 s | |
| Final Elongation | 72 | 5 min | |
| Hold | 12 | ∞ | |

### 3.5.3 Gel eletrophoresis

PCR products were loaded into a 1.5% agarose gel. The gel preparation depends on the size of the gel and the number of samples to run (small gel with 8 or 9 wells, large gel with 11 or 14 wells). The small gel is made with 0,75g of agarose dissolved in 50mL of buffer TAE 1X, and the large one with 1,875g of agarose, dissolved in 125mL of TAE 1X. The TAE 1X was made in the laboratory (recipe in Annex VI). Samples were placed in each gel path together with the buffer in a 9:1 ratio. This buffer is developed for the placement of nucleic acid samples on agarose gels. The Orange dye migrates as a molecule of approximately 50 bp. This allows it to be used as a run front for small nucleic acid fragments. Samples ran at 80V for 40 minutes for the small gel and 1 hour for the large. Images were taken using the UVP software of the ChemiDoc-It Imager and quantified with ImageJ software.

# 4 Results

In this chapter, results obtained from the experiments performed are presented and briefly discussed. They will be divided into three parts on cell treatment and immunohistochemistry, and a part on PCR technique and confirmation of the Fabry mouse genotype. The results of cells treated with Anti-Gb3 antibody for visualisation of this glycolipid are firstly presented, the second part of this chapter represents the results of glycosphingolipid incorporation after treatment with Gb3 and Lyso-Gb3 for 30 minutes, and DGJ and Lyso-Gb3 for 2 hours, the third part analyses the results obtained when comparing the intensity measured only limiting the cell border, or with an ImageJ tool to analyse the intensity at the periphery of the cells. The last part of this chapter corresponds to the analysis and discussion of the results obtained from the PCR. In all images the colour and brightness have been enhanced for signal visibility.

## 4.1 Detection of Anti-Gb3

Propidium iodide is considered an indicator of membrane integrity as it can penetrate through the membrane, allowing the staining of nuclei and cell counting.[28] PI is compatible with direct antibody labelling, and in the present study it was paired with Anti-Gb3 (dilution of 1:100 or 1:200), for subsequent visualisation of this glycosphingolipid.

Figure 4.1 represents the detection of Anti-Gb3, with the image obtained corresponding to a 1:100 dilution of Anti-Gb3 antibody. A), b) and c) represents the staining with PI (blue), Gb3 (green), and the merge of the channels, respectively.

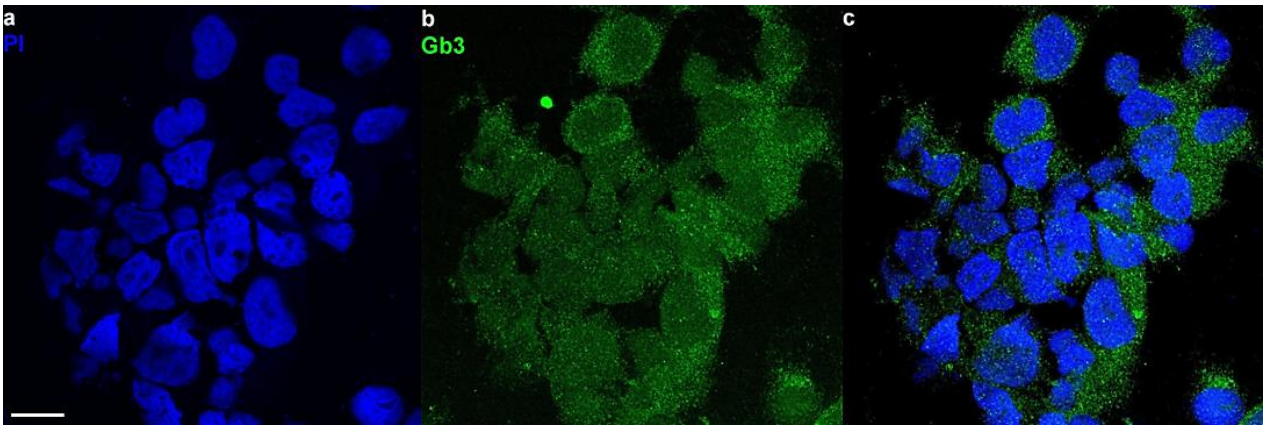


**Figure 4.1** – **Detection of Anti-Gb3.** a) Staining of the cell nuclei by PI staining (blue), b) Detection of the presence of Gb3 (green) and c) Merge of PI and Gb3 channels. The images were viewed with a 40x objective (20µm scale-bar).

## 4.2 Qualitative analysis of the incorporation of glycosphingolipids into HEK cells

As previously mentioned, the present experiments aimed to simulate and evaluate Gb3 and Lyso-Gb3 accumulation in a HEK cellular model. The treatment described in 3.2.3 was performed. The images captured by Confocal FV1000 and Confocal LSM900 were analysed as described in 3.4, with some parameters adjusted to improve the image quality and to make the comparison with the control. Fluorophores are separated by splitting an image into individual channels that represent each signal. The channel that detects the Gb3 signal is selected to determine the *region of interest* (ROIs).

The processed image then undergoes further analysis using the ImageJ tool “particle analysis” with adjustable size parameters. It was necessary to define which parameter was going to be used to determine what was considered a cell. To do so, the outline of each cell nuclei dyed with PI was manually contoured and the area of that ROI was measured, in pixels. The completion of particle analysis results in saving each cell as an ROI. By logging each ROI, the location, shape, and size of a cell are available. Using the average parameter for the contoured nuclei, PI staining area close to this value was defined as a cell.

### 4.2.1 Gb3 accumulation for 30 minutes

Images were taken of distinct regions of Gb3 treated cells in the 543nm (Propidium Iodide) and 488nm (for Gb3, using a secondary antibody Anti-mousse 488) channels.

DMSO is often used in cell treatment since it has low toxicity and does not affect cell growth. [29,30] Its use as a control for the treatments as it serves as a dilution vehicle for the respective drugs.

The set of images was captured in a stack. The selection criterion for each slice of each stacked image was based on the median plan that allowed quantifying a cut where the visualisation of the nuclei was clearer. This plan varies from cell to cell depending on its spatial arrangement and the cut or section made under the microscope. After the direct application of the criteria, the image of the selected plan is chosen for subsequent analysis and quantification of each treatment. All stack images are represented in Annex I.I.

Control images of the Gb3 treatment of the PI and Gb3 channels and their merge are shown in Figure 4.2a), b) and c) respectively. It was not possible to detect a signal with the same parameters in the case of the negative control. The dilution of the Anti-Gb3 antibody was 1:200.

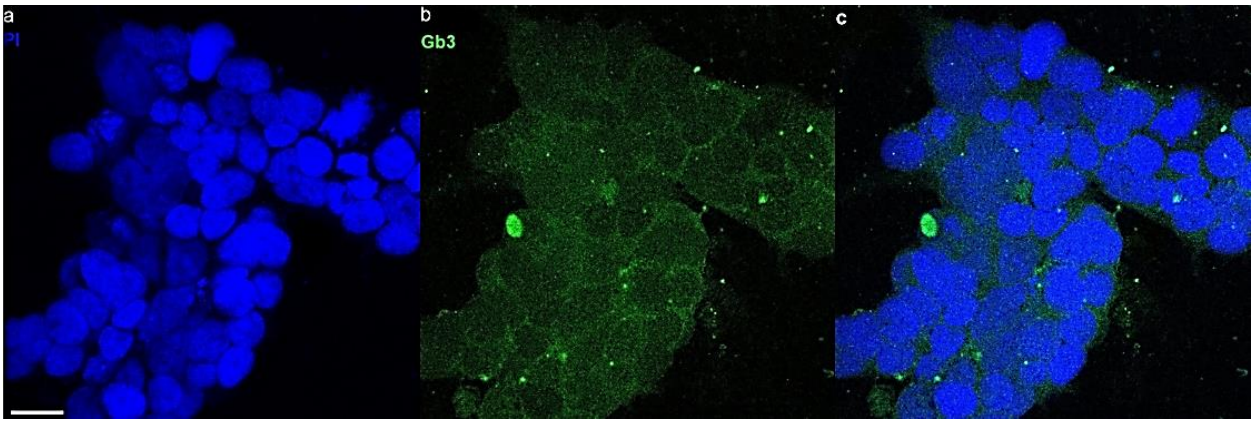


**Figure 4.2 - Control to 30-minute treatment with Gb3.** a) HEK cells counterstained with PI (blue) to detect the nuclei, b) Gb3 signal (green) and c) Merge of PI and Gb3 channel. The images were viewed with a 40x objective (20µm scale-bar).

Two images were obtained corresponding to the treatment with Gb3 for 30 minutes. The most representative image is in Figure 4.3a), b) and c), with the PI channel, Gb3 and the merge of the two, respectively, while the other image is shown in Annex I.II

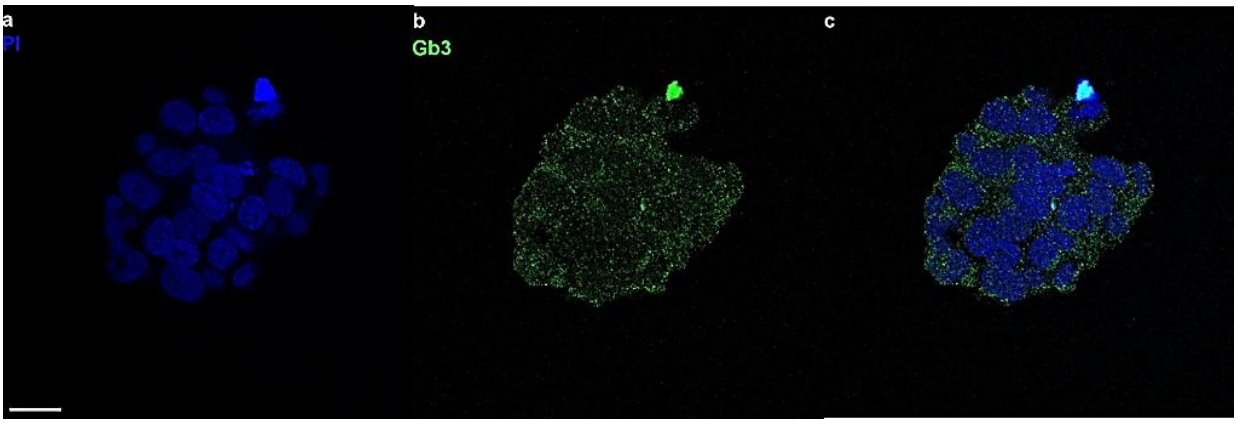


**Figure 4.3** – **Incorporation of Gb3 (30-min treatment)** a) HEK cells stained with PI for nuclei detection (blue), b) Increase in cell signal (green) after incubation of cells with Gb3 and c) Merge of PI and Gb3 channel. All images were viewed with a 40x objective (20µm scale-bar).

As shown in Figure 4.3b), incubation of cells with Gb3 could be detected already after 30 minutes, without alteration at the level of the nuclei.

### 4.2.2 Lyso-Gb3 accumulation for 30 minutes

For treatment with Lyso-Gb3, the dilution of the Anti-Gb3 antibody was 1:100. Five different images were obtained, and the respective controls of images 1, 2 and 3. No Gb3 signal was detected in the negative control, and therefore its subtraction was not necessary. Figure 4.4 represents a control to Lyso-Gb3 treatment, with the respective PI, Gb3 and merge of the two channels. Figure 4.5 represent the most significant obtained image for Lyso-Gb3 treatment. The remaining images obtained can be found in Annex I.III and I.IV.

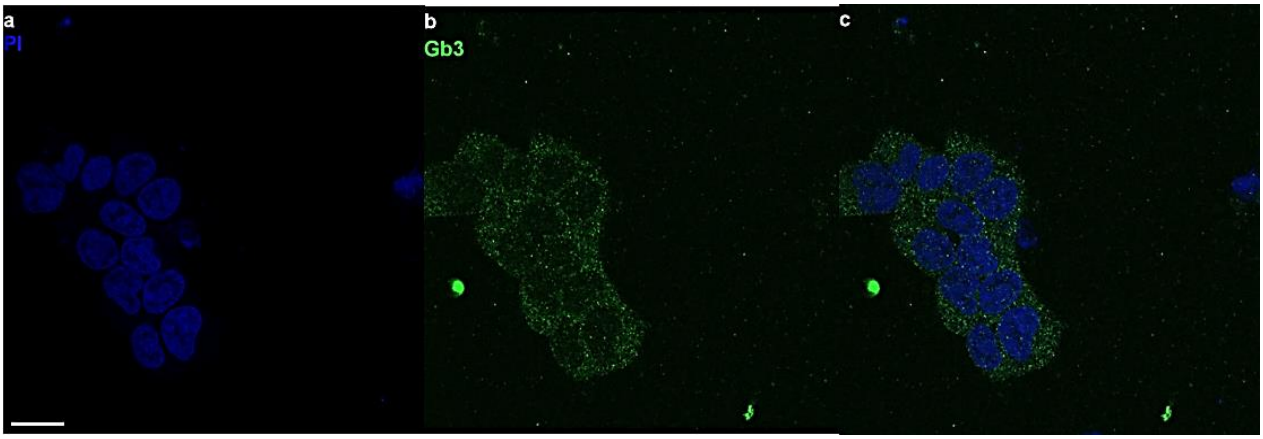


**Figure 4.4 – Control to 30-minute treatment with Lyso-Gb3**.a) HEK cells counterstained with PI (blue) to detect the nuclei, b) Gb3 signal (green) and c) Merge of PI and Gb3 channel. The images were viewed with a 40x objective (20µm scale-bar).

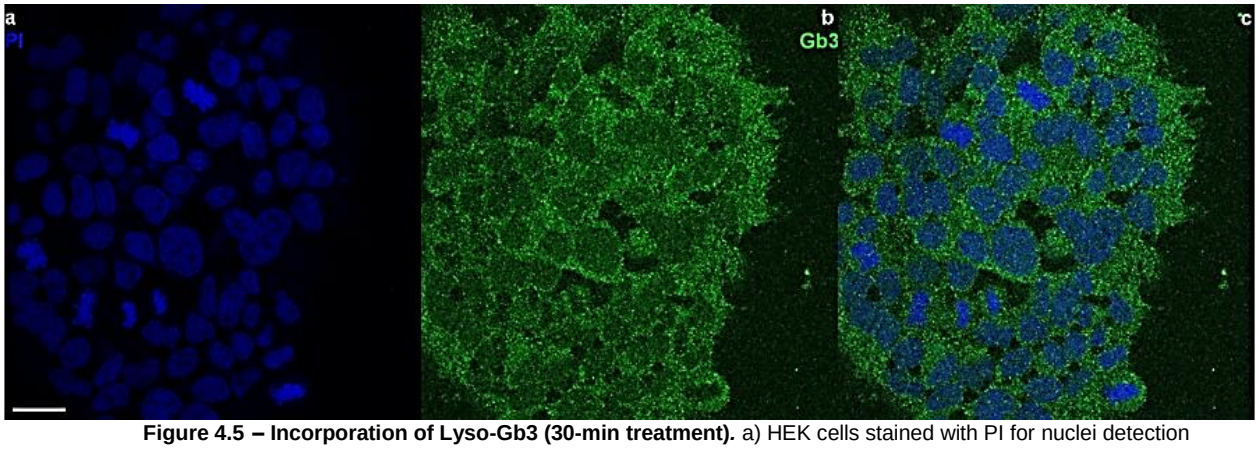


**Figure 4.5 – Incorporation of Lyso-Gb3 (30-min treatment).** a) HEK cells stained with PI for nuclei detection (blue), b) Increase in cell signal (green) after incubation of cells with Lyso-Gb3 and c) Merge of PI and Gb3 channel. All images were viewed with a 40x objective (20µm scale-bar).

Qualitatively, comparing Figure 4.4b) and 4.5b) it is possible to verify a higher intensity in the treated cells.

### 4.2.3 Control for 2 hours

The control for two-hour Lyso-Gb3 and DGJ treatments was made with DMSO and Anti-Gb3.

The images obtained are represented in Annex I.V. Figure 4.6 shows the image selected as the most representative of the controls. Since a signal was detected with the negative control, it had to be considered, and for that purpose, it was subtracted from each image to eliminate the respective signal.

The z=6 plane was chosen, with its respective Gb3 and PI channels represented in Figures 4.6a) and 4.6b).

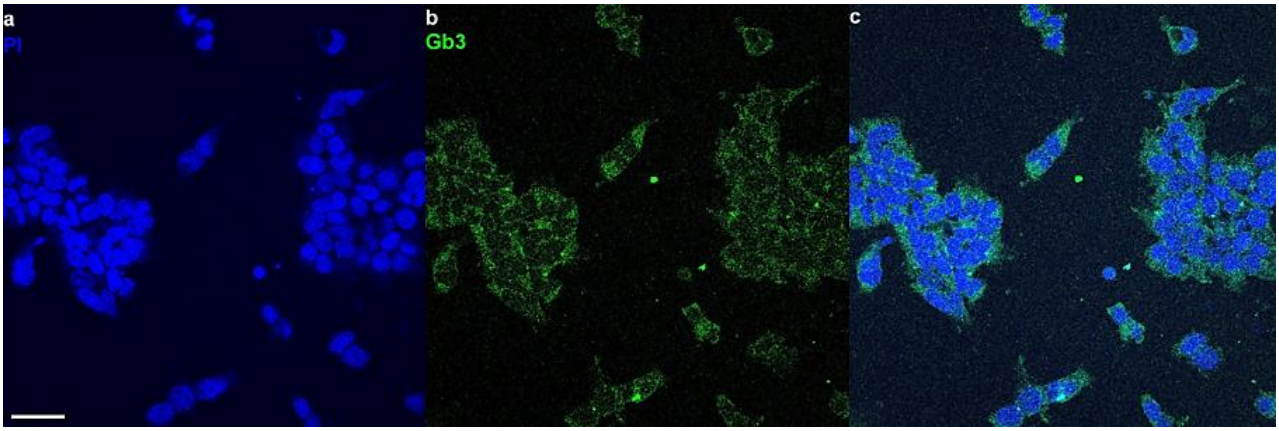


**Figure 4.6 – Control to 2-hour treatment**. a) HEK cells counterstained with PI (blue) to detect the nuclei, b) Gb3 signal (green) and c) Merge of PI and Gb3 channel. The images were viewed with a 40x objective (20μm scale-bar).

### 4.2.4 DGJ treatment for 2 hours

Gb3 accumulation was studied after treatment with DGJ for 2 hours, an α-galactosidase A enzyme inhibiting drug.

The most representative image obtained is represented in Figure 4.7, with the respective PI and Gb3 channels. Annex I.VI contains the remaining images obtained. Since a signal was detected with the negative control, it had to be considered, and for that purpose, it was subtracted from each image to eliminate the respective signal.

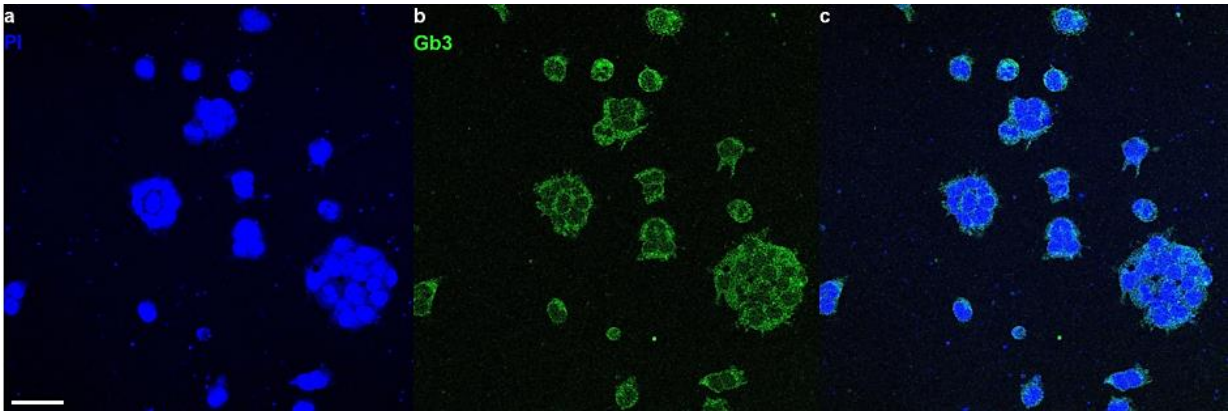


**Figure 4.7 - Gb3 accumulation (2-hour treatment with DGJ).** a) PI channel to visualise the nuclei, b) Gb3 channel do detect this glycolipid and c) Merge of both channels. The images were viewed with a 40x objective (20μm scale-bar).

On a qualitative level, comparing the images of the Gb3 channel obtained after treatment with DGJ with those used as a control (subchapter 4.2.3 and Annex I.V), it is possible to see a greater accumulation of Gb3, given the higher intensity in the respective channel, when compared with the intensity levels of the same channel in the respective control.

### 4.2.5 Lyso-Gb3 accumulation for 2 hours

The last treatment was a 2-hour treatment with Lyso-Gb3 to assess and quantify the incorporation of this glycolipid.

Four different images were obtained for the Lyso-Gb3 treatment. Annex I.VII contains the stack images of the treatments carried out with Lyso-Gb3, representing in Figure 4.8 the most representative image obtained, with the respective PI and Gb3 channels. Since a signal was detected with the negative control, it had to be considered, and for that purpose, it was subtracted from each image to eliminate the respective signal.

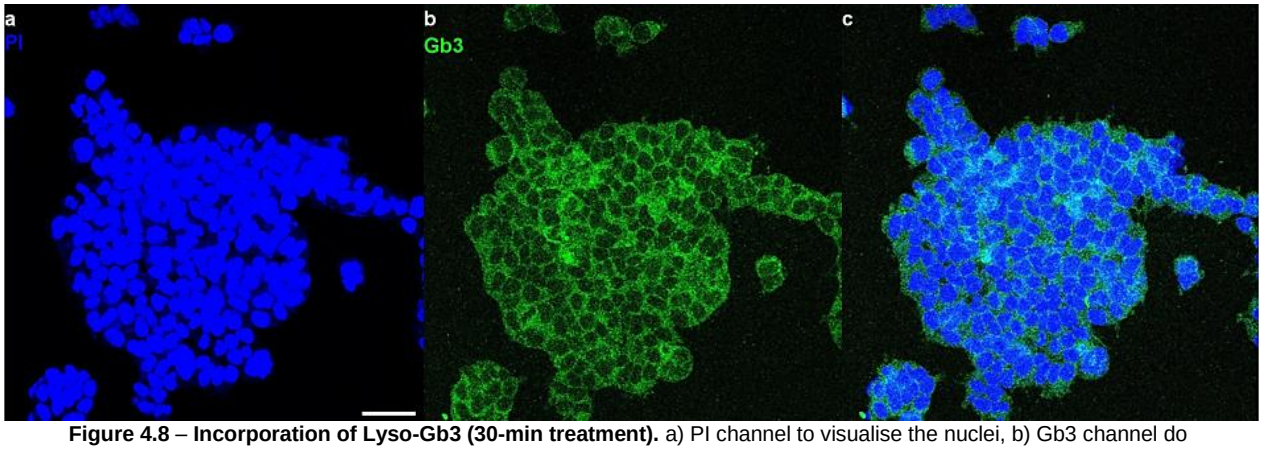


**Figure 4.8** – **Incorporation of Lyso-Gb3 (30-min treatment).** a) PI channel to visualise the nuclei, b) Gb3 channel do detect Lyso-Gb3 and c) Merge of both channels. The images were viewed with a 40x objective (20µm scale-bar).

Similarly to the treatment with DGJ, an increase in fluorescence intensity compared to the control is also observed when treated with Lyso-Gb3 for two hours.

## 4.3 Quantification of glycosphingolipids in a cellular model

The accumulation of Gb3 and Lyso-Gb3 was quantified according to its intensity by comparing the different treatments with the control, for the two different times analysed, 30 minutes or 2 hours.

For an equivalent comparison between the different treatments and the one taken as a control, all images were analysed raw and unaltered. To quantify the intensity of each treatment and compare it with the control, the intensity value of the background was checked and subtracted from the whole image. Afterwards, each cell was manually defined as ROI and its *mean grey value* was measured.

With the values obtained, graphs were drawn to compare these intensity values between the treatments and the control, and statistical analysis was performed using *GraphPad Prism 8* software.

First are the results obtained for treatment with Gb3 (Figure 4.9) and Lyso-Gb3 (Figure 4.10), for the respective treatment time of 30 minutes. Next, are the graphs obtained for the 2-hour treatment with DGJ or Lyso-Gb3, Figures 4.11 and 4.12, respectively.

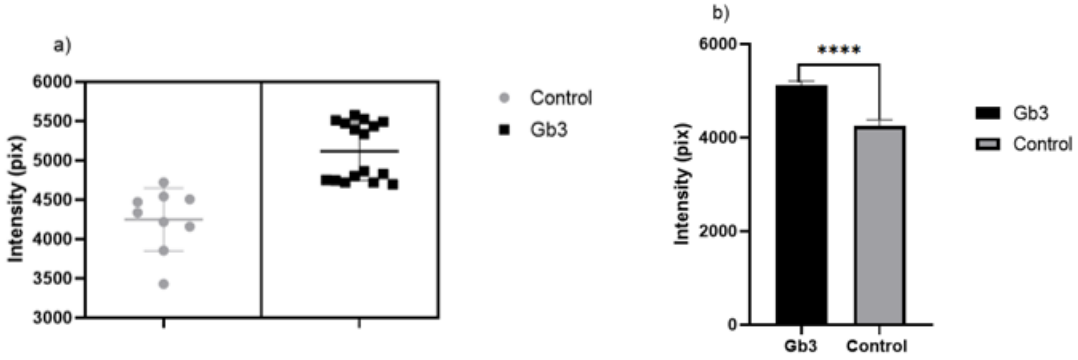


**Figure 4.9** - **Quantitative analysis of Gb3 incorporation levels for the 30-minute treatment**. a) Comparison of the intensity levels measured in pixels between the control and Gb3, after treatment with Gb3 for 30 minutes. b) Quantification and statistical analysis of the intensity levels of the samples. Data are presented as the mean ± SEM. ****p < 0.0001 by unpaired *t test.*

From the analysis of Figure 4.9, the intensity measured in cells subjected to Gb3 treatment is higher when compared to control cells and the accumulation of this glycolipid is immediately visible after 30 minutes. All samples followed a normal distribution by the normality tests performed, as well as presenting distinct variances.

The *p value* obtained (p<0.0001) allows us to infer that there are significant differences in the intensity levels of Gb3 and untreated cells. Gb3 treatment increases the concentration of this glycolipid in cells, incorporating directly into the cells.

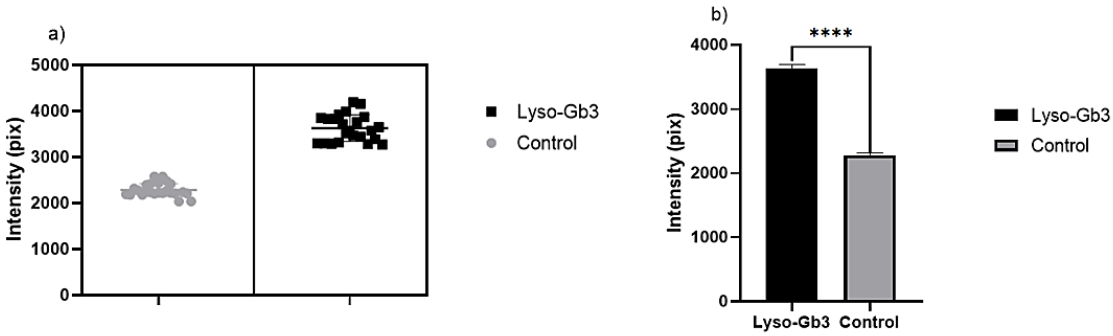


**Figure 4.10 - Quantitative analysis of Lyso-Gb3 incorporation levels for the 30-minute treatment.** a) Comparison of the intensity levels measured in pixels between the control and treatment with Lyso-Gb3 for 30 minutes. b) Quantification of the intensity levels of the respective samples. Data are presented as the mean ± SEM. ****p < 0.0001 by unpaired *t test*.

With the data in Figure 4.10 it is possible to see that there is also an increase in intensity for all the samples treated with Lyso-Gb3 after 30 minutes. Compared to the control samples, the increase in intensity after treatment (p<0.0001) is significant, corresponding to the

accumulation of this glycolipid in the respective samples. Annex II represents the graph comparing each of the images obtained from the Lyso-Gb3 treatment with its control.

The results obtained for the 2-hour treatment with DGJ or Lyso-Gb3 were analysed and are shown below. Annex III contains the graphs with the results obtained from the comparison between each image treated with Lyso-Gb3 or DGJ and the control for each of these treatments.

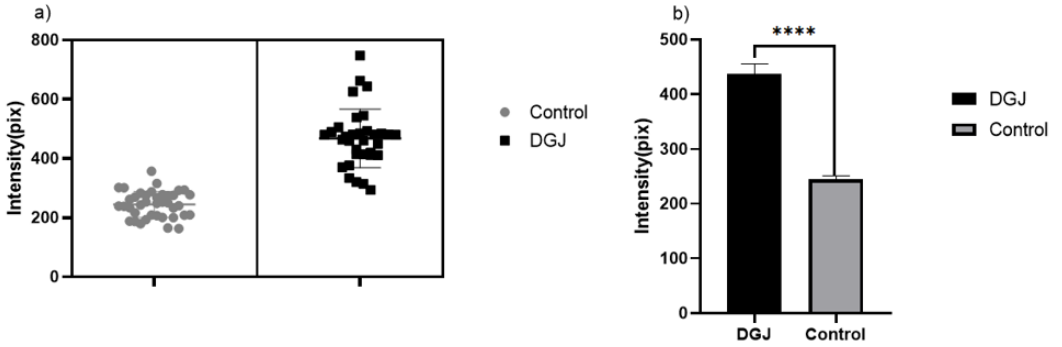


**Figure 4.11 – Quantitative analysis of Gb3 incorporation levels for the 2-hours treatment.** a) Comparison of the intensity levels between control and the DGJ treatment for 2 hours. b) Quantification of the intensity levels of the respective samples. Data are presented as the mean ± SEM. ****p < 0.0001 by unpaired *t test*.

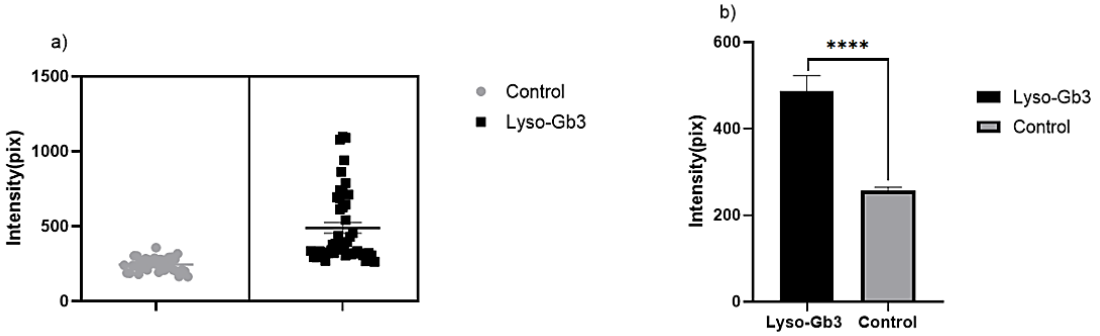


**Figure 4.12 - Quantitative analysis of Lyso-Gb3 incorporation levels for the 2-hour treatment.** a) Comparison of the intensity levels between control and the Lyso-Gb3 treatment for 2 hours. b) Quantification of the intensity levels of the respective samples. Data are presented as the mean ± SEM. ****p < 0.0001 by unpaired *t test*.

By Shapiro-Wilk test, all values for the two 2-hour treatments followed a normal distribution. Unpaired *t tests* were used to assess the differences in intensity levels between the two treatments and the control. For both Lyso-Gb3 and DGJ, there were significant differences when comparing the intensity levels with the control *(*p<0.0001 for Lyso-Gb3 and DGJ).

It was also studied where the greatest accumulation of this glycosphingolipid occurred. To do this, an analysis of the intensity around each cell was performed; using a software imaging tool "*enlarge*", a 10-pixel (for the 30 minutes treatment images) or 5-pixel (for the 2 hours treatment images) zoom was taken around each cell and the intensity levels were compared. This was done for all treatments: Gb3, DGJ and Lyso-Gb3.

Always the same cells were compared, and the images were worked on raw and without any adjustment. With the values obtained, graphs were drawn to compare these intensity values between the images with or without enlargement, and statistical analysis was performed using *GraphPad Prism 8* software.

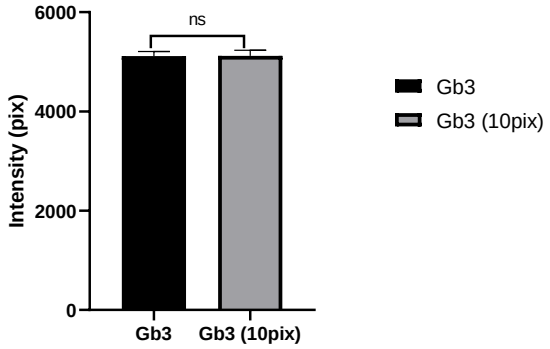


**Figure 4.13** – **Gb3 location**. Quantification of the intensity levels between Gb3 and Gb3(10pix). Data are presented as the mean ± SEM. *ns* by unpaired *t test*.

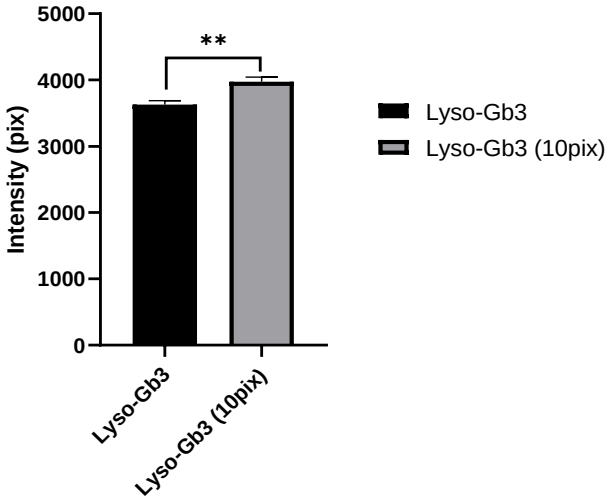


**Figure 4.14 – Lyso-Gb3 location.** Quantification of the intensity levels between the Lyso-Gb3 and Lyso-Gb3 (10pix). Data are presented as the mean ± SEM. **p <0.001 to 0.01 by unpaired *t test*.

Then, for the two-hour Lyso-Gb3 and DGJ treatment, a 5 pixel enlarge was taken.

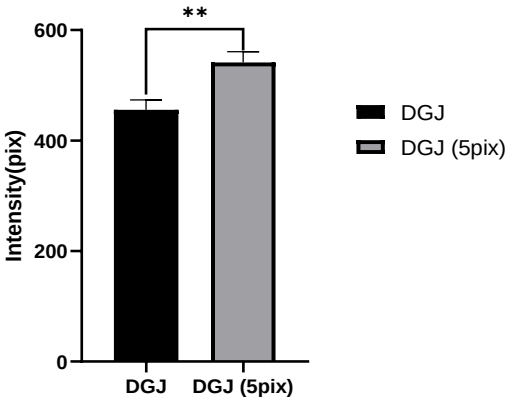


**Figure 4.15** – **Gb3 Location.** Quantification of the intensity levels between DGJ and DGJ (5pix). Data are presented as the mean ± SEM. **p <0.001 to 0.01 by unpaired *t test.*

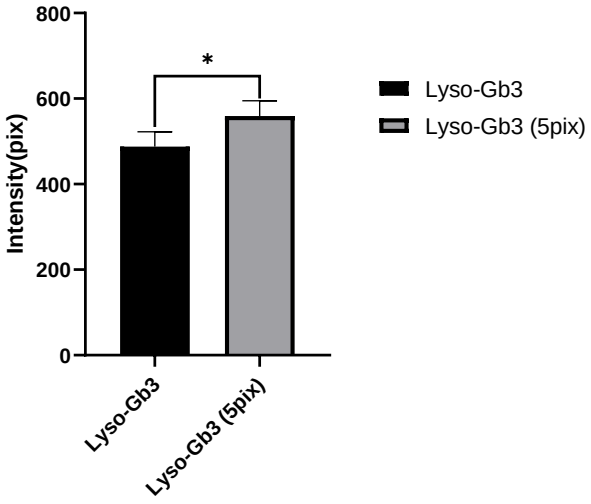


**Figure 4.16 – Lyso-Gb3 location**. Quantification of the intensity levels between Lyso-Gb3 and Lyso-Gb3 (5pix). Data are presented as the mean ± SEM. *p 0.01 to 0.05 by unpaired *t test*.

By the analysis of Figure 4.13, regarding the treatment with Gb3 for 30 minutes, no differences were demonstrated, and no conclusions can be drawn as to the cellular location of this lipid.

The graph in Figure 4.14, concerning the treatment with Lyso-Gb3 for 30 minutes, shows that there are significant differences with the enlargement of 10 pixels. Given these results, it is possible to infer the location of Lyso-Gb3.

Differences were seen in the two-hour treatments (DGJ and Lyso-Gb3), however, taking 5 pixels of enlargement (graphs in Figures 4.15 and 4.16).

Further experiments and attempts would be necessary to prove where this glycolipid is located.

The results of the different treatments were compared. For 30 minutes, the levels of Lyso-Gb3 intensity were compared with Gb3, and for 2 hours, the levels of Lyso-Gb3 intensity were compared with DGJ. The graphs in Figure 4.17 show the results obtained.

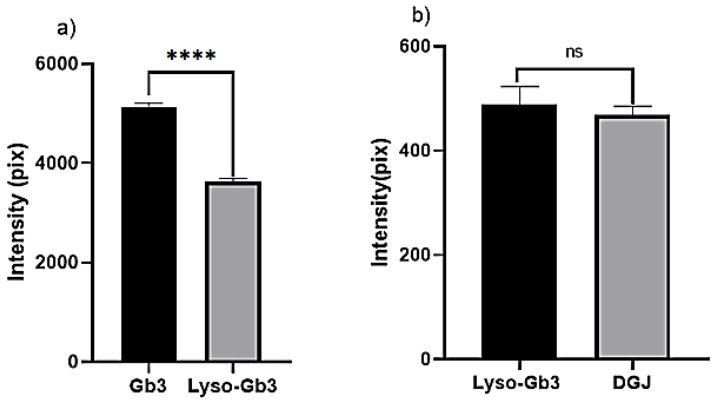


**Figure 4.17** - **Treatment comparison.** Quantification of intensity levels between a) 30 minutes Lyso-Gb3 treatment with Gb3 and b) 2h Lyso-Gb3 treatment with DGJ. Data are presented as the mean ± SEM. ****p < 0.0001 and *ns* by unpaired *t test.*

There are significant differences when comparing Gb3 and Lyso-Gb3 intensity levels (*p value*<0.0001); these results are not following the literature, where Lyso-Gb3 levels are an order of magnitude higher than Gb3 levels.[31] Regarding the results obtained when comparing DGJ with Lyso-Gb3, no significant differences were found. The individual comparison between each treatment with Lyso-Gb3 and DGJ is in Annexes IV.

The intensity levels of the treatment with Lyso-Gb3 were compared for two different times, 30 minutes, and 2 hours, to understand after what time the accumulation of this glycolipid was greater. The mean ratio of the intensity levels of the results obtained with Lyso-Gb3 to the respective controls was calculated. The graph in Figure 4.18 shows and compares these values.

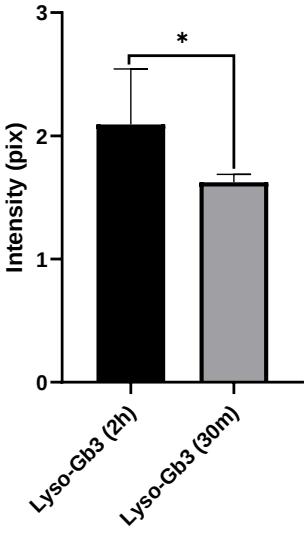


**Figure 4.18** - **Differences between treatments over time.** Quantification of the ratio of intensity levels between Lyso-Gb3 treatments of 30 minutes and 2 hours with their respective controls. Data are presented as the mean ± SEM. *p 0.01 to 0.05 by unpaired *t test.*

By analysing the graph in Figure 4.18, the treatment with Lyso-Gb3 of two hours showed higher levels of intensity compared with that made only for 30 minutes.

Finally, the differences between the control (made with DMSO and with Anti-Gb3 added) and the negative control (made with DMEM only and without Anti-Gb3 added) were checked. The bar graphs in Figures 4.19a) and 4.19b) illustrate the results obtained for the quantitative analysis between the control and negative control of 30 minutes and 2 hours, respectively.

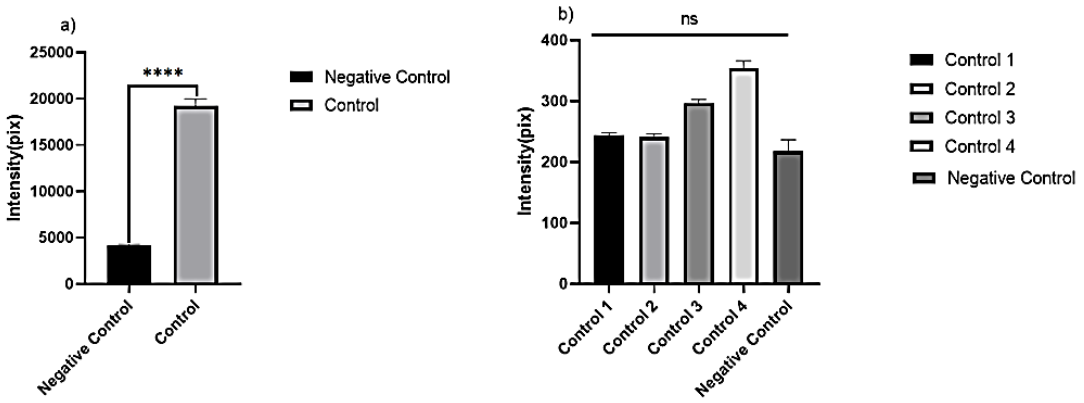


**Figure 4.19** - **Differences between the control and the negative control.** a) Comparison and quantification between the control and the negative control for the 30-minute treatment. b) Comparison and quantification between the four controls and the negative control for the 2-hour treatment. Data are presented as the mean ± SEM. ***p 0.0001 to 0.001 and *ns* by unpaired *t test*.

## 4.4 PCR Results

The objective of the PCR technique performed was the confirmation of the genome of Fabry model mice. The technique was performed according to the procedure described in 3.5 and with the conditions explained in 3.5.2. Before performing the PCR technique, some conditions had to be put in place, such as the ideal dilution of the enzyme Taq Polymerase (Annex V).

Confirmation of a KO mice is given by the presence of a band at 202 bp, just as a WT mice is confirmed by the appearance of the band at 295 bp. The negative control was made with the same amounts of MasterMix, but without the addition of the DNA sample, with the remaining 6µL being replaced by water. The positive control was initially made by a heterozygous mouse, with the appearance of the two bands, KO and WT (Sample 24). Subsequently, the positive control was replaced by a mouse already known to be WT or KO, just to ensure that the PCR was well performed. The amount of DNA was measured using NanoDrop One System by Thermo Scientific to assess the relationship between the intensity of the bands obtained by PCR and the amount of DNA in the sample. These values, as well as the classification of each mouse, can be found in Annex VII.

The Figures 4.20 – 4.24 show the results obtained for the samples analysed.

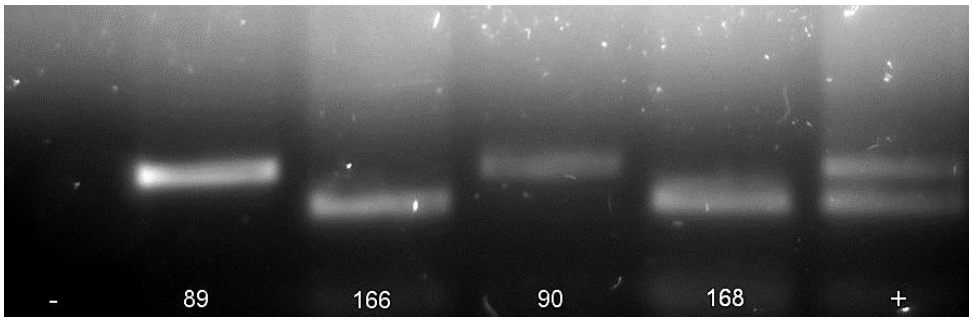


**Figure 4.20** – **PCR Results (1).** Determination of samples 89 (WT), 166 (KO), 90 (WT), 168 (KO), negative control (-) and positive control (sample 24, heterozygous) by PCR.

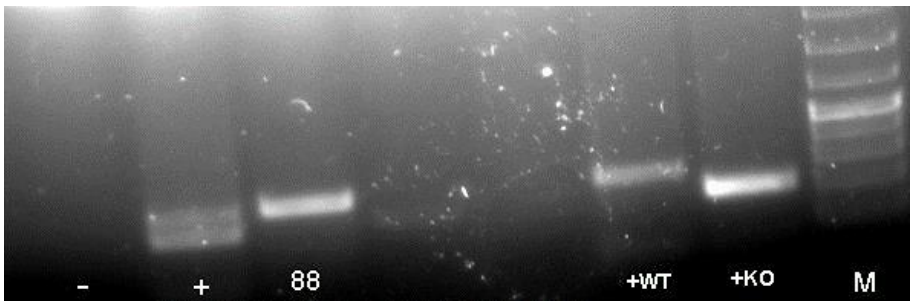


**Figure 4.21** - **PCR Results (2).** Determination of samples 88 (WT), negative control (-), positive control (sample 24, heterozygous), one positive control for WT (+WT), one for KO (+KO), and DNA-Marker by PCR.

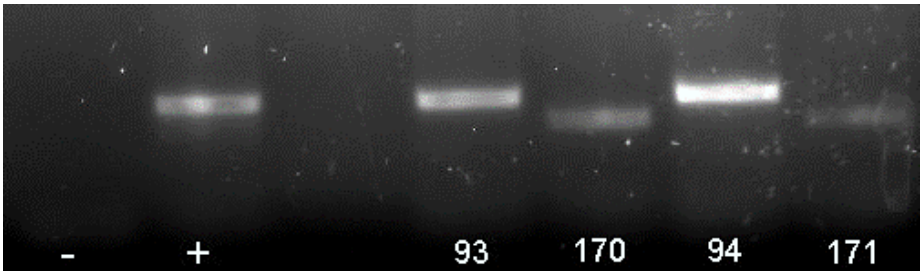


**Figure 4.22** – **PCR Results (3).** Determination of samples 93 (WT), 170 (KO), 94 (WT), 171 (KO), the positive control of WT (+) and the negative control (-) by PCR.

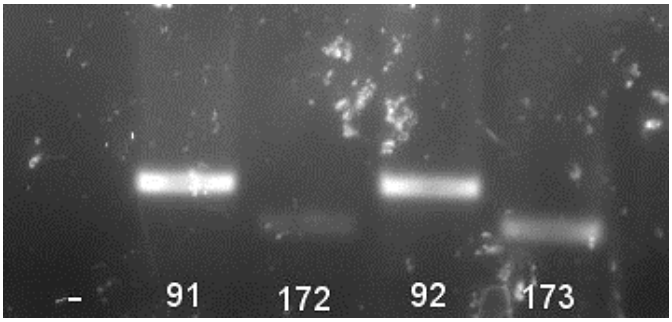


**Figure 4.23 - PCR Results (4).** Determination of samples 91 (WT), 172 (KO), 92 (WT), 173 (KO) and the negative control (-) by PCR.

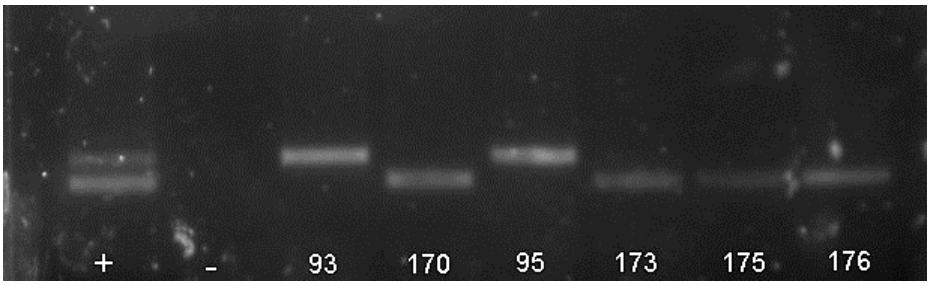


**Figure 4.24** – **PCR Results (6).** Determination of samples 93 (WT), 170 (KO), 95 (WT), 173 (KO), 175 (KO), 176 (KO), the positive control for WT and KO (+) and the negative control (-) by PCR.

By analysis of the images previously presented, the intensity of the bands corresponding to the WT is higher than the bands of the KO. This result is as expected since the amount of DNA from WT is higher than the amount of DNA from KO, and the intensity of the bands is proportional to the amount of DNA present, as the bands of mice 88, 91, 92 and 94 are the most intense and it was precisely in these that the largest amounts of DNA were distinguished (Table 8.2). However, this was not confirmed with other animals where, even with large amounts of DNA, the intensity of the bands was not highly expressed (example, mouse 176). Pipetting errors or errors in performing the technique may have influenced the running of these bands and consequently the decrease in their intensity.

# 5 Discussion

Glycosphingolipids are constituents of the plasma membrane responsible for modulating membrane-receptor activity and transport processes. The propensity of Gb3 to localise in the cell membrane in Fabry disease may be related to its physiologic function.[32] Several experiments have demonstrated that Gb3 is present in endothelium tissues, the cytoplasm of endothelial cells and cell surface, varying according to the cell cycle.[8,33,34]

The results obtained for the Gb3, Lyso-Gb3 and DGJ treatments show differences when compared with the respective controls. These differences are expressed by analysis of the graphs in Figures 4.9, 4.10, 4.11 and 4.12. The results are as expected since treatment with Gb3 or Lyso-Gb3 promotes the direct incorporation of these glycosphingolipids. The treatment with DGJ, at the concentration at which it was used (the same used by Asano *et al*. 2000), promotes the inhibition of the α-Gal A enzyme and consequently the accumulation of Gb3 in the cell endothelium and lysosomal compartments.[35,36] However, the threshold values at which DGJ acts as an inhibitor must be considered, since DGJ also works as a pharmacological chaperone that binds to enzyme α-Gal A and stabilizes it, promoting its activity values.[37]

The results obtained when the software imaging tool "*enlarge*" was used to study the cellular location of Gb3. The graph in Figure 4.13 shows that there were no significant differences, so it is not possible to conclude on the exact location of this glycolipid. More experiments and a higher *n* would be necessary to be able to infer the location where this glycolipid accumulates. On the other hand, the results obtained after treatment with Lyso-Gb3 (Figure 4.14) show significant differences when a larger cell area is taken ($p<0.05$ in all cases). For the two-hour treatment with DGJ and Lyso-Gb3, the location of these glycosphingolipids was also studied by taking an enlargement of 5 pixels. Differences were found for both treatments (*p value* of 0.0014 and 0.0106, for DGJ and Lyso-Gb3, respectively). Given these results, it appears that the accumulation of glycosphingolipids occurs more at the cell periphery, however, to corroborate such a statement, a larger number of samples would have to be analysed.

Although, for all treatments, it must be considered that certain factors can influence the intensity levels measured. In some preparations, it was necessary to exclude some cells because they had saturating levels, and the intensity levels measured did not correspond to the true ones.

The graph in Figure 4.17a) compares the intensity levels obtained from the Gb3 treatment with those obtained from the Lyso-Gb3 treatment for 30 minutes. It was found that the levels of the treatment with Gb3 are significantly higher than with Lyso-Gb3 (*p value* < 0.0001). From the literature, it would be expected that Lyso-Gb3 levels would be higher by approximately 1 order of magnitude than Gb3 levels.[31] The results obtained are not by the literature. The

background of the images analysed may have been different between the two treatments, and consequently influenced the intensity levels.

The intensity values between the two-hour, Lyso-Gb3 and DGJ treatments, were also compared (Figure 4.17b). No differences were found between the two treatments. This result is as expected since both treatments, at the concentrations used, promote glycolipid incorporation.

The intensity levels obtained for the Lyso-Gb3 treatment for 30 minutes were analysed with the same treatment for two hours (Figure 4.18). The intensity levels of the 2-hour treatment are higher and the difference with the 30-minute treatment is significant (*p value* of 0.0203). These results are as expected since treatment with Lyso-Gb3 for two hours promotes a greater accumulation of this glycolipid compared to the treatment performed for only 30 minutes. Although two different microscopes, Confocal FV1000 for 30 minutes and Confocal LSM900 for 2 hours, were used, each one was used for the respective control and treatment (a whole set), so this factor was not a source of difference.

Finally, the differences between the 30-minute treatment control with Gb3 and Lyso-Gb3, with their respective negative control, and the same for the two-hour treatment with Lyso-Gb3 and DGJ were verified (Figure 4.19). The control was always made with DMSO, an incorporating carrier of Gb3 and Lyso-Gb3, and with the addition of Anti-Gb3. The negative control was made with DMEM and without the addition of Antibody. For the 30-minute treatment, significant differences were observed between the control and the negative control. The result was as expected since the intensity of the negative control should have been much lower than the control. For the 2-hour treatment, no significant differences were found.

In general, the results obtained were as expected. Significant differences were found between the treatments and the respective control, with higher levels of intensity for treatments either by direct incorporation of glycosphingolipids (treatment with Gb3 or Lyso-Gb3), or by indirect incorporation (treatment with DGJ), which, at the concentration used, acts as an inhibitor of the α-galactose enzyme, and increases Gb3 levels.

Regarding the cellular location of Gb3 and Lyso-Gb3, by data obtained from the literature, it would be expected to find greater accumulation at the peripheral level and cell membrane, since these glycolipids are involved in membrane processes, such as recognition and interaction with other molecules, is in epithelial tissues and is located on the cell surface, in particular domains called lipid rafts.

Concerning the results obtained by the PCR technique (Chapter 4.4), it was possible to genotype the animals and to corroborate that the animals used in the experiments were of the correct genotype.

# 6 Conclusion and Future Work

The main objective of this project was to quantify globotriaosylceramide accumulation in a model of HEK cells. Gb3 is assumed to be the main offending metabolite, although the mechanism by which its accumulation leads to the multisystem disorder of Fabry disease is not known. It has traditionally been stated that Gb3 is stored in lysosomes and that mechanically or by some other process these lipid-laden lysosomes cause disease.[38] The accumulation of this glycolipid is due to the deficient, or non-existent, activity of enzyme α-galactosidase, which is responsible for its metabolization.

In this work, the efficacy of Gb3 in treating cells in culture was studied to verify if it was detectable and could be subsequently used in the cell model.

Immunohistochemistry performed on different tissues from Fabry patients revealed the presence of Gb3. However, its deacylated form, Lyso-Gb3, was shown to have a higher concentration in the same tissues, thus emerging as a potential primary biomarker for Fabry disease.[31] This glycolipid is accumulated in the cell membrane and cytoplasm of endothelial cells. Its presence in these areas is consistent with their respective function.

Glycosphingolipids like globotriaosylceramide (Gb3) have been identified as key regulators of a wide variety of cellular processes, including proliferation, differentiation, adhesion, autophagy, inflammation, migration, and angiogenesis. Like other glycosphingolipids, Gb3 resides preferentially in specialized membrane domains termed lipid rafts. In the cell membrane, lipid rafts act as platforms for cellular or exogenous proteins with different functions, including the shuttling of molecules on the cell surface, organization of cell signal transduction pathways and the formation of pathological forms of proteins.[39,40] Alterations in lipid rafts compromise downstream signalling, survival, differentiation, and its disruption is associated with the onset of neurodegenerative diseases. However, the effects that glycosphingolipid accumulation may have on the dynamics of lipid rafts are not yet known. Labilloy *et al.* postulated that α-Gal A silencing and subsequent accumulation of neutral glycosphingolipids at the plasma membrane would impact how proteins interact with lipid rafts and potentially induce changes in the oligomerization of raft-associated proteins and affect the present ion channels. These changes may have an impact on raft-mediated signal transduction in Fabry disease.[40,41]

Another characteristic of globotriaosylceramide is that, in proximal tubular epithelial cells (PTECs), it can act as a facilitator for the uptake of filtered proteins such as albumin and low-molecular weight (LMW) proteins filtered into the primary urine.[42]

Two distinct therapies are currently accepted for Fabry disease – Enzyme Replacement Therapy and Chaperone Therapy. While both improve quality of life and alleviate some symptoms, they do not inhibit the progression of the disease.[43,44] As there is still no sufficiently effective therapy for the treatment of FD, it would be interesting to study the detection and

location of Gb3, as, given its diverse functionality, it could contribute to the development of new and more specific therapies.

In the future, markers of other cellular structures could be used to verify the accumulation of this glycolipid in other cellular zones, such as nuclear and endoplasmic reticulum markers.

For the work previously carried out, it would be necessary to repeat the experiments to benefit the data analysis and ensure the veracity of the conclusions drawn, as well as to bridge some differences between the treatment of the cells and their visualisation.

For a future work, immunohistochemical techniques could be performed with the primary antibody used (Anti-Gb3) in the Fabry disease model mice to which the DNA was genotyped. Another target of study would be to understand more deeply the effect that the accumulation of glycolipids in the plasma membrane has on the interaction of proteins with lipid rafts and the effects on the ion channels present in this structure. It would be interesting to know how the elimination of these glycosphingolipids from the tissues where it accumulates takes place. Since the organs where the highest concentration of Gb3 and Lyso-Gb3 is detected and how the accumulation process occurs are already known, it would be beneficial to understand what the mechanism of their elimination is, under which conditions it occurs and the factors that influence it, in situations of inhibition or reduced activity of α-galactosidase A.

The last part of this work consisted of the confirmation of the genome of Fabry model animals. Initially, it was necessary to make some adjustments to the technique, such as studying the best Taq-Polymerase dilution and changing some reagents, until it could be carried out in the best way and obtain the desired results.

The results obtained were as expected, as the respective bands were obtained according to whether the animal was WT or KO, and with intensity proportional to the amount of DNA contained in the sample.

Finally, this work allowed the study of the accumulation of the glycolipid characteristic of Fabry disease in a cellular model subjected to different treatments. These results will give continuity to the studies already initiated on glycosphingolipid accumulation and its effects on ASIC1a channel regulation, a mediator of the ERK signalling pathway.

Hopefully, the small steps taken, the shortcomings found in the experiments performed, and the possibilities considered will pave the way for new and improved future therapies for Fabry disease.

# 7 References


1. Rozenfeld PA, Ceci R, Roa N, Kisinovsky I. *The Continuous Challenge of Diagnosing patients with Fabry disease in Argentina*. *J Inborn Errors Metab Screen*. 2015;3(1900):232640981561380. doi:10.1177/2326409815613806

2. Baehner F, Kampmann C, Whybra C, Miebach E, Wiethoff CM, Beck M. Enzyme replacement therapy in heterozygous females with Fabry disease: Results of a phase IIIB study. *J Inherit Metab Dis*. 2003;26(7):617-627. doi:10.1023/B:BOLI.0000005658.14563.77

3. Sunder-Plassmann G, Födinger M, Kain R. Fabry disease. *National Kidney Foundation's Primer on Kidney Diseases, Sixth Edition*. Published online 2013:381-387. doi:10.1016/B978-1-4557-4617-0.00044-3

4. Lukas J, Giese AK, Markoff A, et al. Functional Characterisation of Alpha-Galactosidase A Mutations as a Basis for a New Classification System in Fabry Disease. *PLoS Genet*. 2013;9(8). doi:10.1371/journal.pgen.1003632

5. Chu XP, Papasian CJ, Wang JQ, Xiong ZG. Modulation of acid-sensing ion channels: Molecular mechanisms and therapeutic potential. *Int J Physiol Pathophysiol Pharmacol*. 2011;3(4):288-309.

6. Garman SC, Garboczi DN. The molecular defect leading to fabry disease: Structure of human α-galactosidase. *J Mol Biol*. 2004;337(2):319-335. doi:10.1016/j.jmb.2004.01.035

7. Azevedo O, Gago MF, Miltenberger-Miltenyi G, et al. Natural history of the late-onset phenotype of Fabry disease due to the p.F113L mutation. *Mol Genet Metab Rep*. 2020;22(November 2019):100565. doi:10.1016/j.ymgmr.2020.100565

8. Celi AB, Goldstein J, Rosato-Siri MV, Pinto A. Role of Globotriaosylceramide in Physiology and Pathology. *Front Mol Biosci*. 2022;9(February):1-20. doi:10.3389/fmolb.2022.813637

9. Disease F. *Gb 3 and Lyso-Gb 3 and Fabry Disease INSIDE THIS ISSUE*. www.matreya.com

10. Ortiz A, Germain DP, Desnick RJ, et al. Fabry disease revisited: Management and treatment recommendations for adult patients. *Mol Genet Metab*. 2018;123(4):416-427. doi:10.1016/j.ymgme.2018.02.014

11. Calvo JH. *Nefropatía de La Enfermedad de Fabry*. http://www.hgmd.cf.ac.uk/ac/index.php , consulted in 24/06/2022.

12. Kahn P. Anderson Fabry disease: a histopathological study of three cases with observations on the mechanism of production of pain. *J Neurol Neurosurg Psychiatry*. 1973;36(6):1053-1062. doi:10.1136/JNNP.36.6.1053

13. Gayathri N, Yasha T, Kanjalkar M, et al. Fabry's disease: An ultrastructural study of nerve biopsy. *Ann Indian Acad Neurol*. 2008;11(3):182-184. doi:10.4103/0972-2327.42939

14. Deval E, Gasull X, Noël J, et al. Acid-Sensing Ion Channels (ASICs): Pharmacology and implication in pain. *Pharmacol Ther*. 2010;128(3):549-558. doi:10.1016/j.pharmthera.2010.08.006

15. Gründer S, Chen X. *Review Article Structure, Function, and Pharmacology of Acid-Sensing Ion Channels (ASICs): Focus on ASIC1a*. Vol 2.; 2010. www.ijppp.org/IJPPP1002001

16. Benarroch EE. Acid-sensing cation channels: Structure, function, and pathophysiologic implications. *Neurology*. 2014;82(7):628-635. doi:10.1212/WNL.0000000000000134

17. Castellanos LCS, Rozenfeld P, Gatto RG, Reisin RC, Uchitel OD, Weissmann C. Upregulation of ASIC1a channels in an in vitro model of Fabry disease. *Neurochem Int*. 2020;140. doi:10.1016/j.neuint.2020.104824

18. Hofmann L, Hose D, Grießhammer A, et al. Characterization of small fiber pathology in a mouse model of Fabry disease. Published online 2018. doi:10.7554/eLife.39300.001

19. Duan B, Wu LJ, Yu YQ, et al. Upregulation of acid-sensing ion channel ASIC1a in spinal dorsal horn neurons contributes to inflammatory pain hypersensitivity. *Journal of Neuroscience*. 2007;27(41):11139-11148. doi:10.1523/JNEUROSCI.3364-07.2007

20. Slanzi A, Iannoto G, Rossi B, Zenaro E, Constantin G. In vitro Models of Neurodegenerative Diseases. *Front Cell Dev Biol*. 2020;8. doi:10.3389/fcell.2020.00328

21. Graudejus O, Ponce Wong R, Varghese N, Wagner S, Morrison B. Bridging the gap between in vivo and in vitro research: Reproducing in vitro the mechanical and electrical environment of cells in vivo. *Front Cell Neurosci*. 2018;12. doi:10.3389/conf.fncel.2018.38.00069

22. Thomas P, Smart TG. HEK293 cell line: A vehicle for the expression of recombinant proteins. *J Pharmacol Toxicol Methods*. 2005;51(3 SPEC. ISS.):187-200. doi:10.1016/j.vascn.2004.08.014

23. Dumont J, Euwart D, Mei B, Estes S, Kshirsagar R. Human cell lines for biopharmaceutical manufacturing: history, status, and future perspectives. *Crit Rev Biotechnol*. 2016;36(6):1110-1122. doi:10.3109/07388551.2015.1084266

24. Bangari DS, Ashe KM, Desnick RJ, et al. α-Galactosidase A knockout mice: Progressive organ pathology resembles the type 2 later-onset phenotype of fabry disease. *American Journal of Pathology*. 2015;185(3):651-665. doi:10.1016/j.ajpath.2014.11.004

25. Taguchi A, Maruyama H, Nameta M, et al. A symptomatic Fabry disease mouse model generated by inducing globotriaosylceramide synthesis. *Biochemical Journal*. 2013;456(3):373-383. doi:10.1042/BJ20130825

26. Bleve G, Rizzotti L, Dellaglio F, Torriani S. Development of reverse transcription (RT)-PCR and real-time RT-PCR assays for rapid detection and quantification of viable yeasts and molds contaminating yogurts and pasteurized food products. *Appl Environ Microbiol*. 2003;69(7):4116-4122. doi:10.1128/AEM.69.7.4116-4122.2003

27. Fitzpatrick M. *The Open Lab Book Release 1.0*.; 2021, consulted on 07/09/2022.

28. Rosenberg M, Azevedo NF, Ivask A. Propidium iodide staining underestimates viability of adherent bacterial cells. *Sci Rep*. 2019;9(1). doi:10.1038/s41598-019-42906-3

29. Chen X, Thibeault S. Effect of DMSO concentration, cell density and needle gauge on the viability of cryopreserved cells in three dimensional hyaluronan hydrogel. In: *Proceedings of the Annual International Conference of the IEEE Engineering in Medicine and Biology Society, EMBS*. ; 2013:6228-6231. doi:10.1109/EMBC.2013.6610976

30. Stacey GN, Dowall S. Cryopreservation of Primary Animal Cell Cultures. In: ; 2007:271-281. doi:10.1007/978-1-59745-362-2_19

31. Aerts JM, Groener JE, Kuiper S, et al. *Elevated Globotriaosylsphingosine Is a Hallmark of Fabry Disease*.; 2008. www.pnas.orgcgidoi10.1073pnas.0712309105

32. Hin-Fai Yam G, Bosshard N, Zuber C, Steinmann B, Roth J. Pharmacological chaperone corrects lysosomal storage in Fabry disease caused by trafficking-incompetent variants. Published online 2006. doi:10.1152/ajpcell.00426.2005.-Fabry

33. Morace I, Pilz R, Federico G, et al. Renal globotriaosylceramide facilitates tubular albumin absorption and its inhibition protects against acute kidney injury. *Kidney Int*. 2019;96(2):327-341. doi:10.1016/j.kint.2019.02.010

34. Askari H, Kaneski CR, Semino-Mora C, et al. Cellular and tissue localization of globotriaosylceramide in Fabry disease. *Virchows Arch*. 2007;451(4):823-834. doi:10.1007/s00428-007-0468-6

35. Asano N, Ishii S, Kizu H, et al. In vitro inhibition and intracellular enhancement of lysosomal α- galactosidase a activity in fabry lymphoblasts by 1-deoxygalactonojirimycin and its derivatives. *Eur J Biochem*. 2000;267(13):4179-4186. doi:10.1046/j.1432-1327.2000.01457.x

36. Kanda A, Nakao S, Tsuyama S, Murata F, Kanzaki T. Fabry disease: ultrastructural lectin histochemical analyses of lysosomal deposits. *Virchows Arch*. 2000;436(1):36-42. doi:10.1007/pl00008196

37. Hin-Fai Yam G, Bosshard N, Zuber C, Steinmann B, rgen Roth J. Pharmacological chaperone corrects lysosomal storage in Fabry disease caused by trafficking-incompetent variants. Published online 2006. doi:10.1152/ajpcell.00426.2005.-Fabry

38. Desnick R.J. · Wasserstein M.P. · Banikazemi M. Fabry Disease (α-Galactosidase A Deficiency): Renal Involvement and Enzyme Replacement Therapy. 2021;136:174-192.

39. D A Brown EL. Functions of lipid rafts in biological membranes. *Annu Rev Cell Dev Biol*. Published online 1998.

40. Labilloy A, Youker RT, Bruns JR, et al. Altered dynamics of a lipid raft associated protein in a kidney model of Fabry disease. *Mol Genet Metab*. 2014;111(2):184-192. doi:10.1016/j.ymgme.2013.10.010

41. Brian A. Tsui-Pierchala MEJM and EMJJ. Lipid rafts in neuronal signaling. *Trends Neurosci*. 2022;25(8).

42. Ewers H, Helenius A. Lipid-mediated endocytosis. *Cold Spring Harb Perspect Biol*. 2011;3(8):1-14. doi:10.1101/cshperspect.a004721

43. Schiffmann R, Kopp JB, Iii HAA, et al. *Enzyme Replacement Therapy in Fabry Disease A Randomized Controlled Trial*. https://jamanetwork.com/

44. Weidemann F, Jovanovic A, Herrmann K, Vardarli I. Chaperone Therapy in Fabry Disease. *Int J Mol Sci*. 2022;23(3). doi:10.3390/ijms23031887

# 8 Annexes

## **Annex I –** Stack Images

Annex 1 shows the images obtained in a stack of the different treatments carried out and the control. In all images, the brightness and colour parameters were adjusted for better visualisation of the cells.

### **I.I** Control for 30-minute treatment with Gb3

Figure 8.1 depicts the 6 existing planes of the control stack images for 30 minutes, with a distinction between the nuclei (blue) and the glycolipid (green).

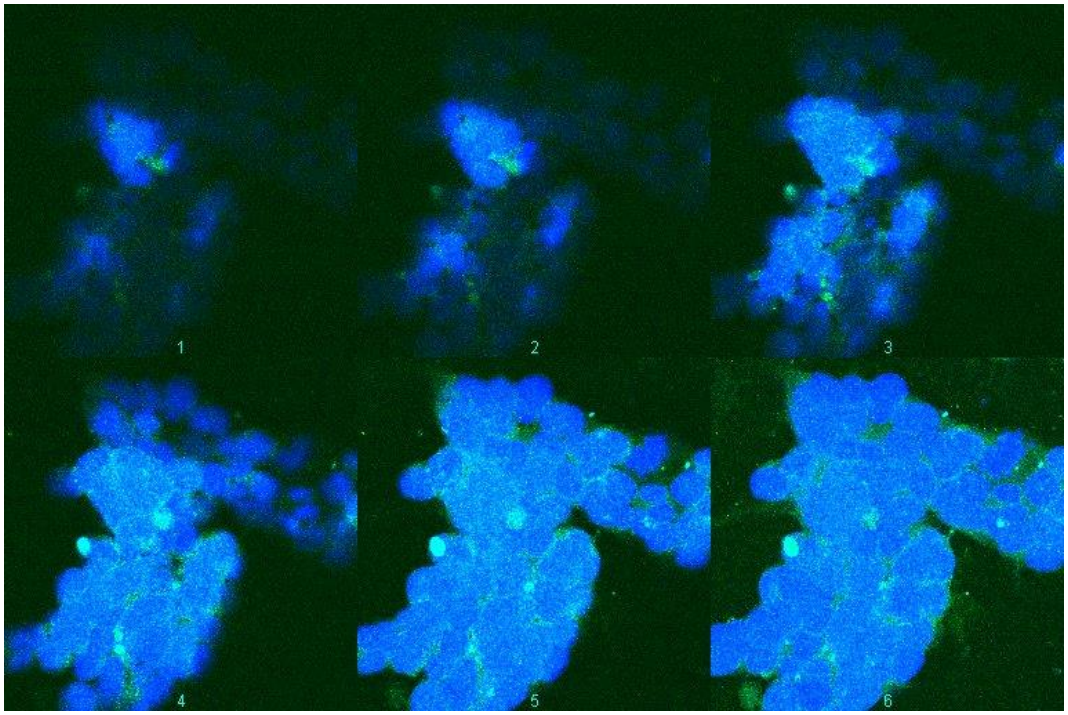


**Figure 8.1– 40x z-stack projections for the control to the 30-minute treatment with Gb3.** 6 different projections. PI and Gb3 channel fusion for nuclei (blue) and Gb3 (green) detection.

### **I.II** 30-minute treatment with Gb3

Two images were obtained corresponding to the treatment with Gb3. The most representative image is represented in Figure 4.3, and the Image 2 is represented in Figure 8.2, with the respective Gb3 and PI channels.

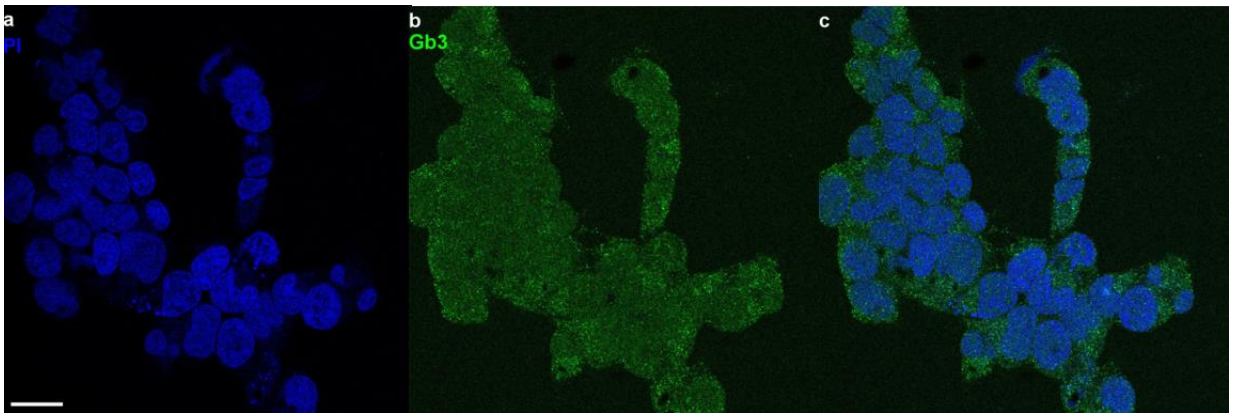


**Figure 8.2 – Image 2 obtained for the 30-minute treatment with Gb3.** a) PI channel to visualise the nuclei, b) Gb3 channel do detect this glycolipid and c) Merge of both channels. The images were viewed with a 40x objective (20µm scale-bar).

## **I.III** Control for 30-minute treatment with Lyso-Gb3

Three different images of the respective control were obtained after treatment with Lyso-Gb3 for 30 minutes, the most representative one being represented in Figure 4.5, and Image 2 and 3 are represented in Figures 8.3 and 8.4.

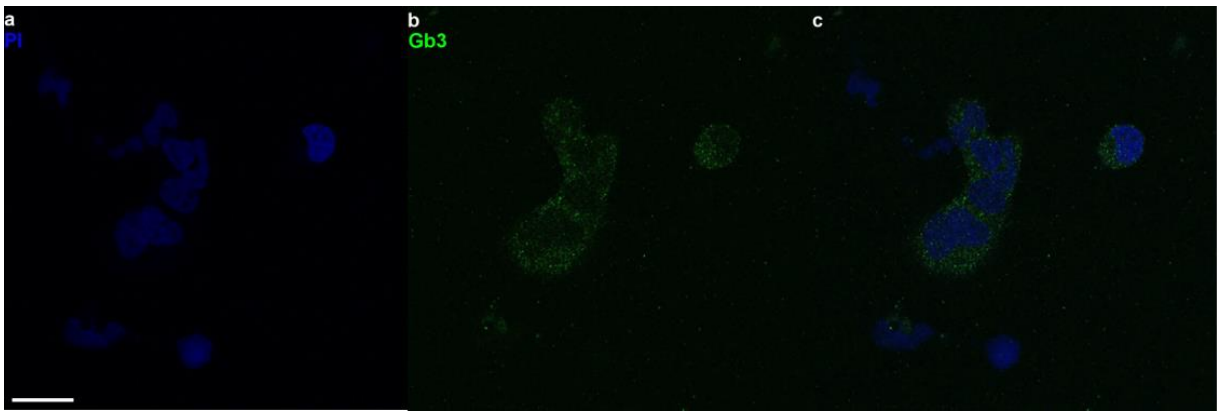


**Figure 8.3 – Control Image 2 from the 30-minute treatment with Gb3.** a) HEK cells counterstained with PI (blue) to detect the nuclei, b) Gb3 signal (green) and c) Merge of PI and Gb3 channel. The images were viewed with a 40x objective (20µm scale-bar).

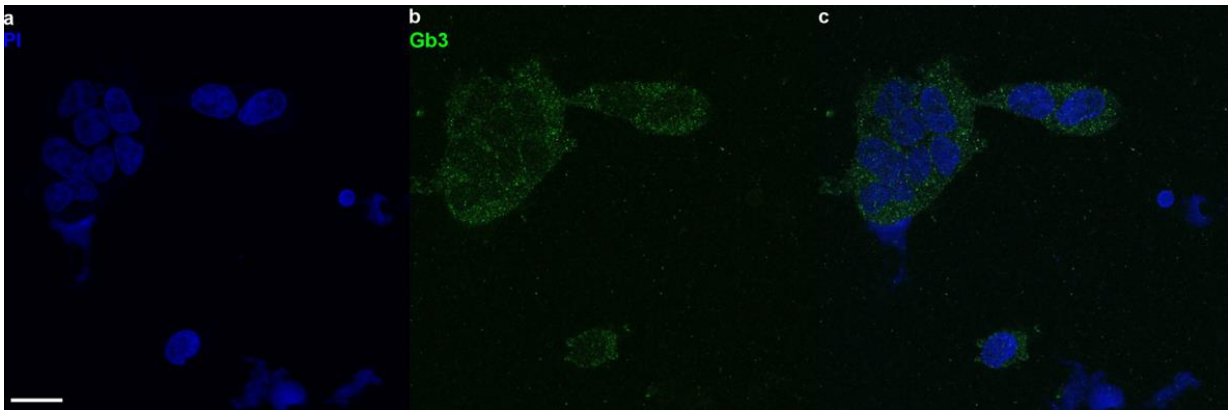


**Figure 8.4 – Control Image 3 from the 30-minute treatment with Gb3.** a) HEK cells counterstained with PI (blue) to detect the nuclei, b) Gb3 signal (green) and c) Merge of PI and Gb3 channel. The images were viewed with a 40x objective (20µm scale-bar).

### **I.IV** 30-minute treatment with Lyso-Gb3

For the treatment with Lyso-Gb3 for 30 minutes, 5 different images were obtained, the most representative being the one shown in Figure 4.5. Figures 8.5-8.8 represent Images 2, 3, 4 and 5, with their respective PI and Gb3 channels.

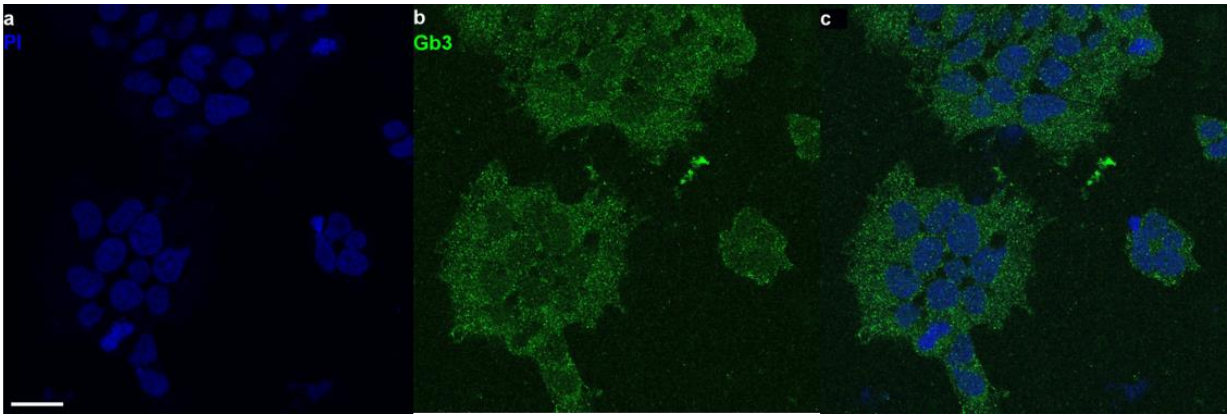


**Figure 8.5** – **Image 2 from the 30-minute treatment with Lyso-Gb3.** a) HEK cells counterstained with PI (blue) to detect the nuclei, b) Gb3 signal (green) and c) Merge of PI and Gb3 channel. The images were viewed with a 40x objective (20μm scale-bar).

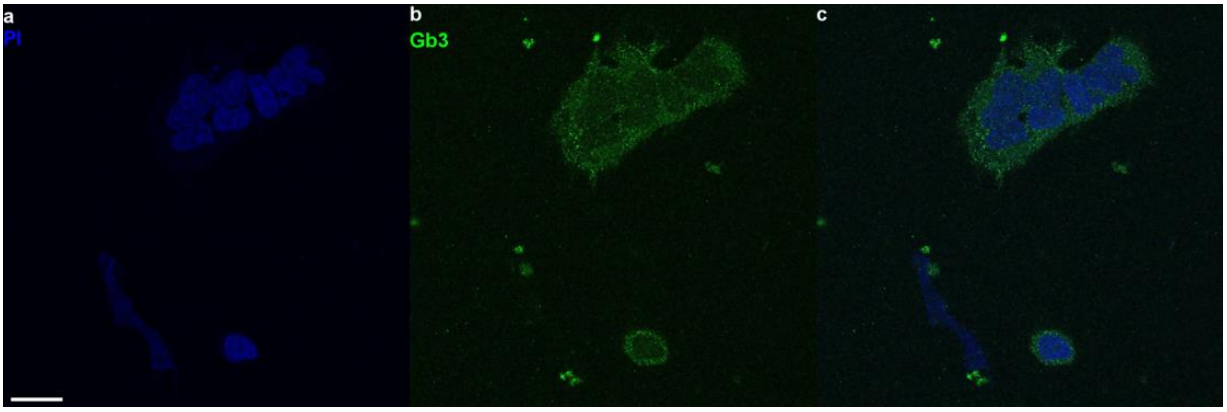


**Figure 8.6** – **Image 3 from the 30-minute treatment with Lyso-Gb3.** a) HEK cells counterstained with PI (blue) to detect the nuclei, b) Gb3 signal (green) and c) Merge of PI and Gb3 channel. The images were viewed with a 40x objective (20μm scale-bar)

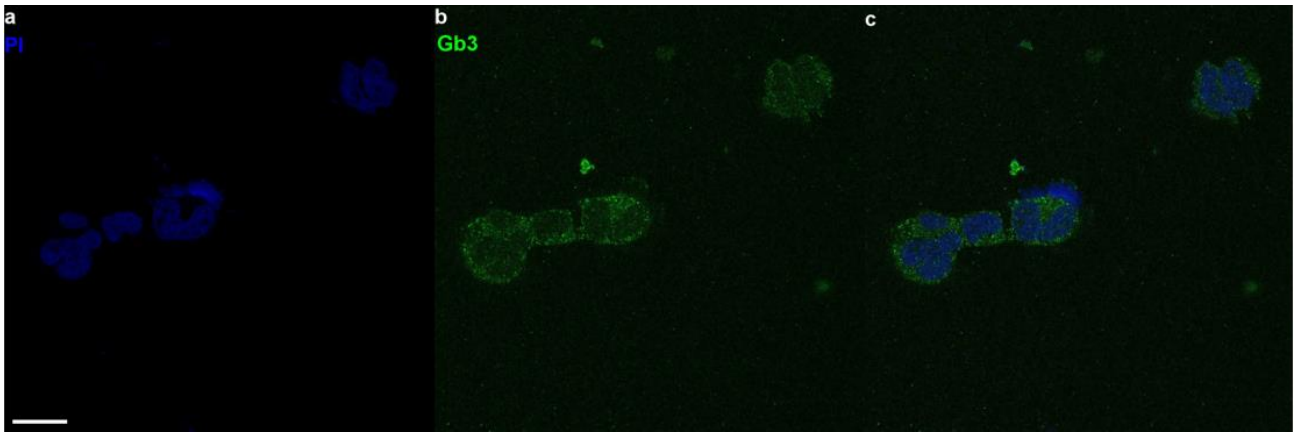


**Figure 8.7** – **Image 4 from the 30-minute treatment with Lyso-Gb3.** a) HEK cells counterstained with PI (blue) to detect the nuclei, b) Gb3 signal (green) and c) Merge of PI and Gb3 channel. The images were viewed with a 40x objective (20µm scale-bar)

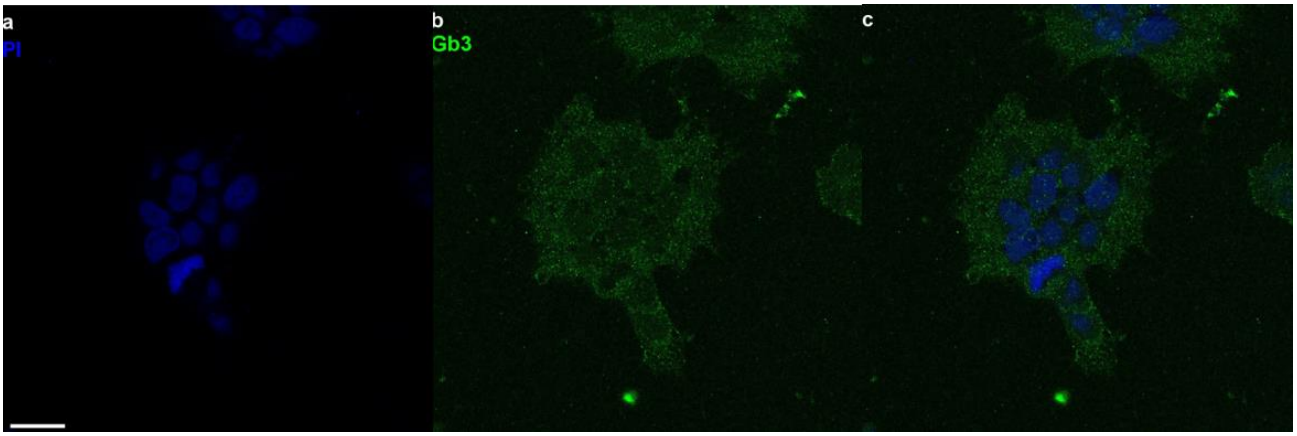


**Figure 8.8 – Image 5 from the 30-minute treatment with Lyso-Gb3.** a) HEK cells counterstained with PI (blue) to detect the nuclei, b) Gb3 signal (green) and c) Merge of PI and Gb3 channel. The images were viewed with a 40x objective (20µm scale-bar)

### **I.V** Control for 2 hours

The images obtained for the control to treatment with Lyso-Gb3 and DGJ are shown in Figures 8.9-8.12.

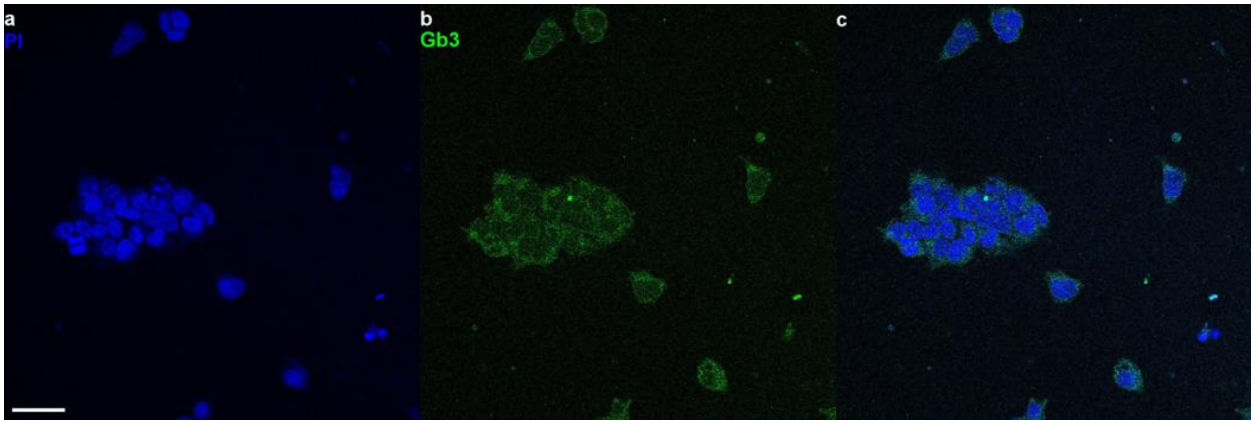


**Figure 8.9 – Control Image 1 from the 2-hour treatment.** a) HEK cells counterstained with PI (blue) to detect the nuclei, b) Gb3 signal (green) and c) Merge of PI and Gb3 channel. The images were viewed with a 40x objective (20µm scale-bar).

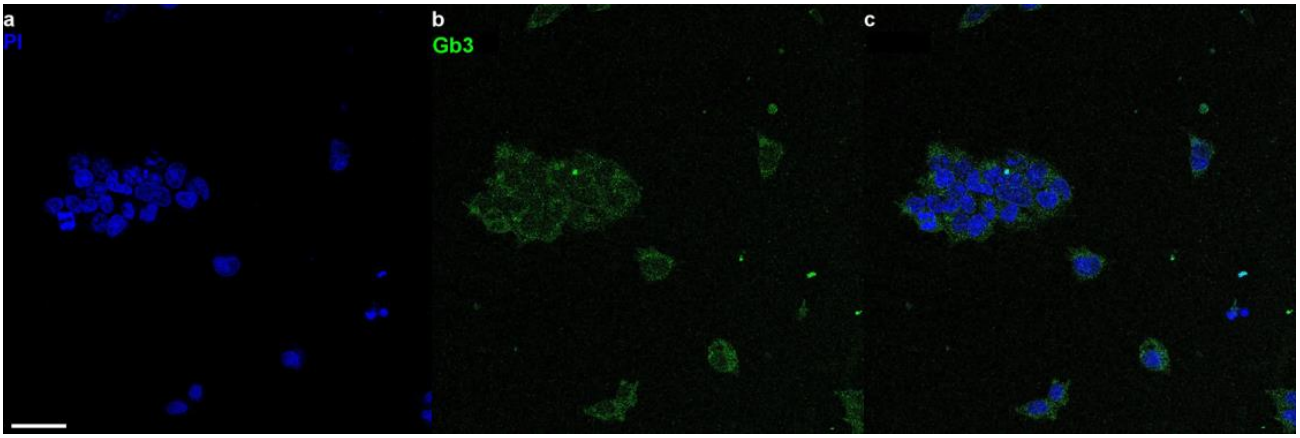


**Figure 8.10 - Control Image 2 from the 2-hour treatment.** a) HEK cells counterstained with PI (blue) to detect the nuclei, b) Gb3 signal (green) and c) Merge of PI and Gb3 channel. The images were viewed with a 40x objective (20µm scale-bar).

The set of stacked images obtained for the control Image 3 and Image 4 to the treatment with DGJ and Lyso-Gb3 are represented in Figures 8.11 and 8.12.

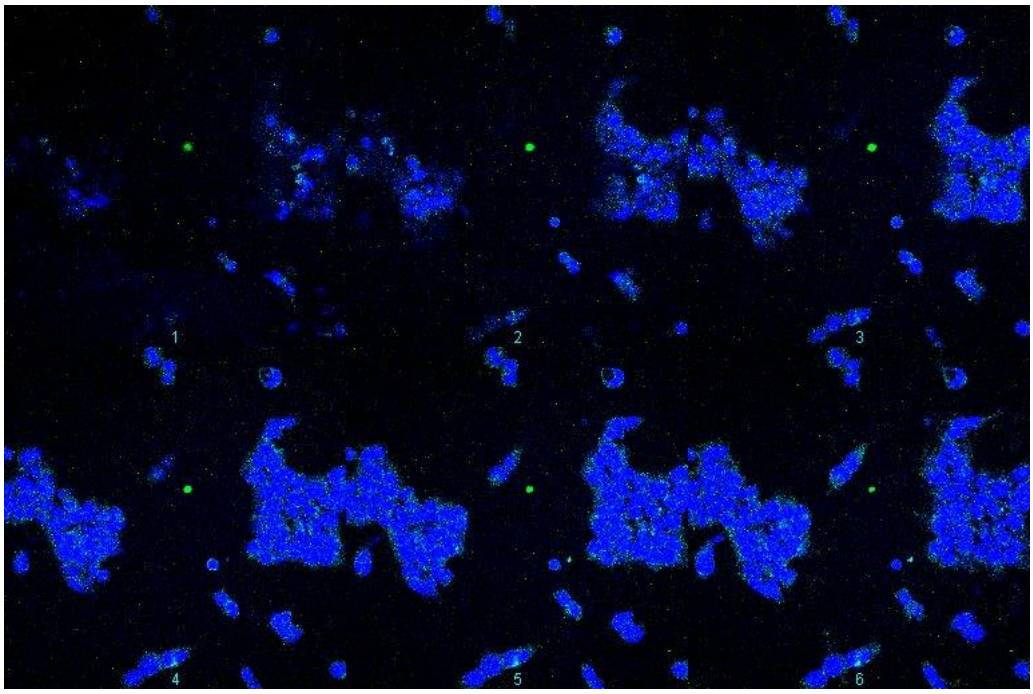


**Figure 8.11 – 40x z-stack projections from the Control Image 3 for 2-hour treatment**. 6 different projections. PI and Gb3 channel fusion for nuclei (blue) and Gb3 (green) detection.

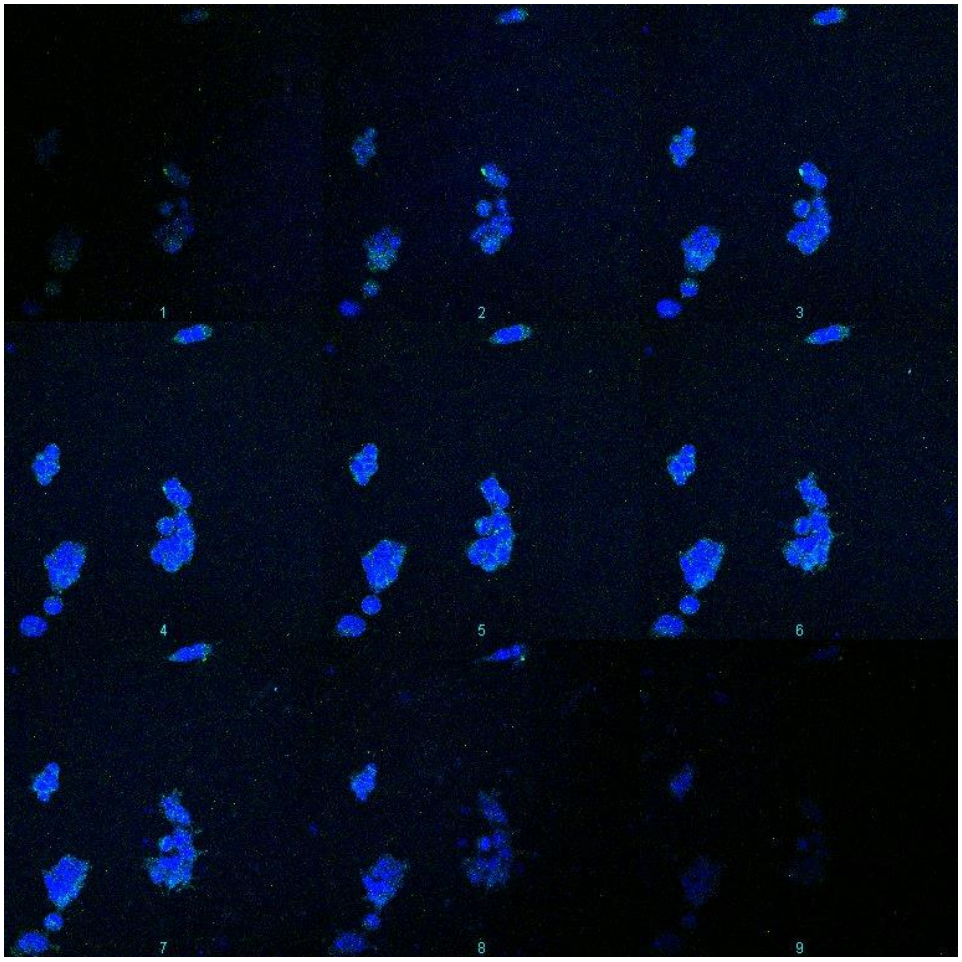


**Figure 8.12 – 40x z-stack projections from the Control Image 4 for the 2-hour treatment.** 9 different projections. PI and Gb3 channel fusion for nuclei (blue) and Gb3 (green) detection.

## **I.VI** DGJ treatment for 2 hours

The Images 1, 3 and 4 for the DGJ treatment are shown in Figures 8.13-8.15. The most representative image is in Figure 4.7.

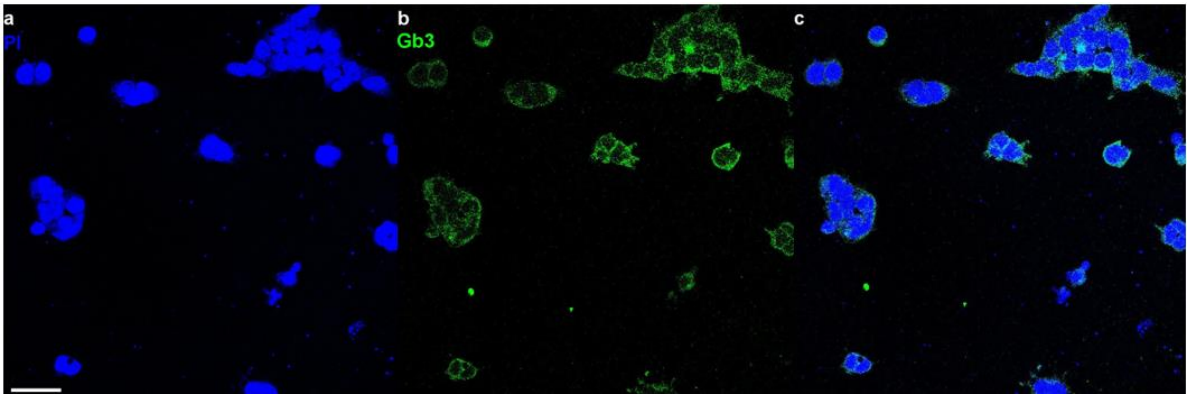


**Figure 8.13** – **Image 1 of 2-hour treatment with DGJ.** a) PI channel to visualise the nuclei, b) Gb3 channel to detect this glycolipid and c) Merge of both channels. The images were viewed with a 40x objective (20μm scale-bar).

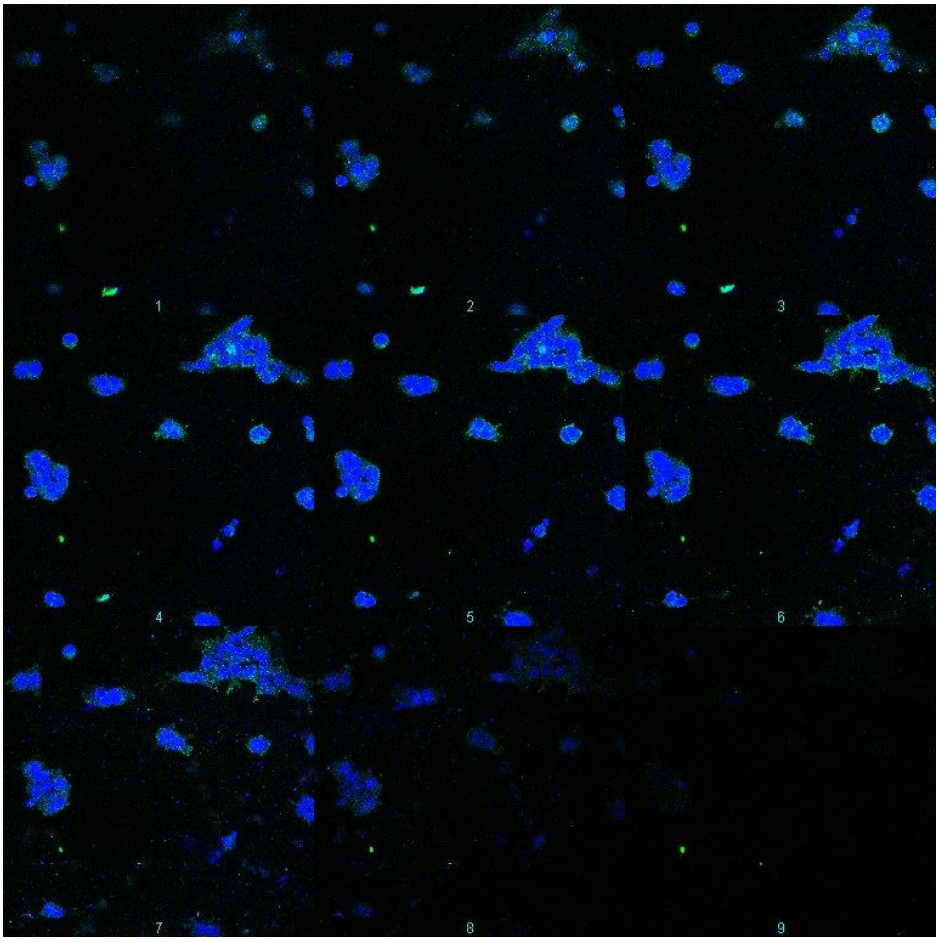


**Figure 8.14 - 40x z-stack projections from the Image 3 of 2-hour treatment with DGJ.** 9 different projections. PI and Gb3 channel fusion for nuclei (blue) and Gb3 (green) detection.

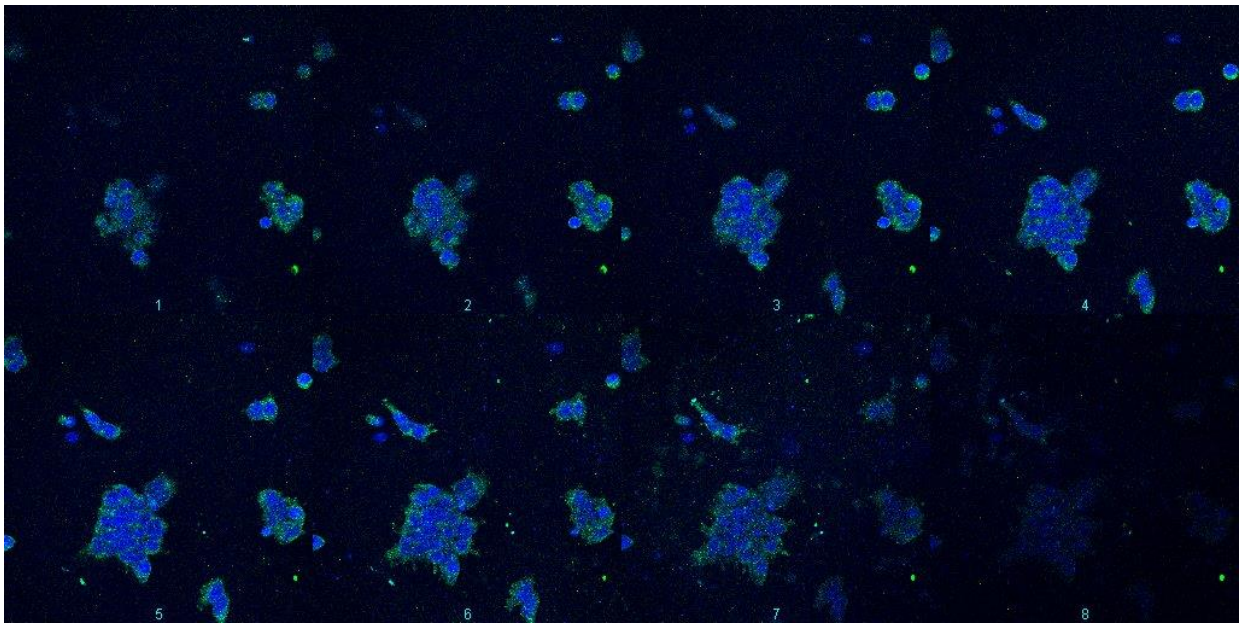


**Figure 8.15 - 40x z-stack projections from the Image 4 of 2-hour treatment with DGJ.** 6 different projections. PI and Gb3 channel fusion for nuclei (blue) and Gb3 (green) detection.

## **I.VII** Lyso-Gb3 treatment for 2 hours

Four different images were obtained for the two-hour treatment with Lyso-Gb3, and Figures 8.16, 8.17 and 8.19 shows the stacked images obtained; Figure 4.8 shows the most representative plane for the two-hour treatment with Lyso-Gb3.

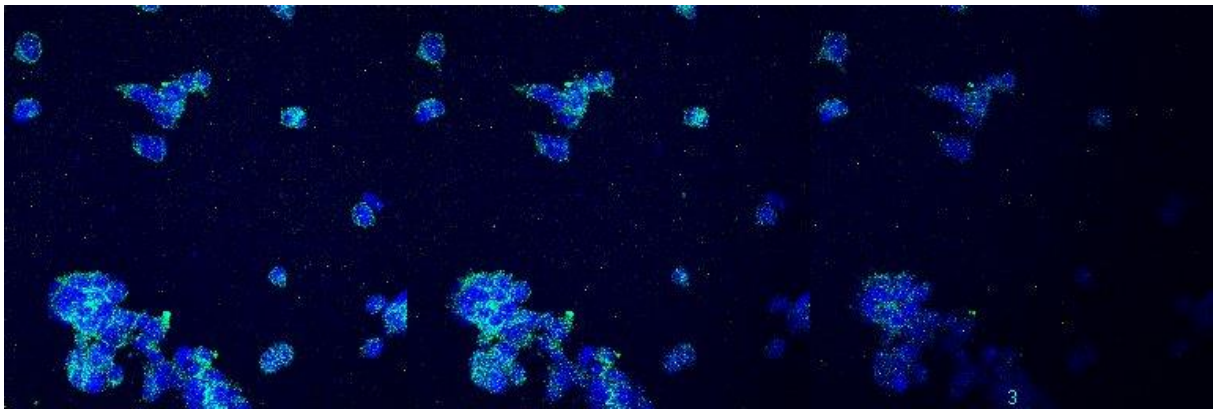


**Figure 8.16 - 40x z-stack projections from the Image 1 of 2-hour treatment with Lyso-Gb3.** 3 different projections. PI and Gb3 channel fusion for nuclei (blue) and Gb3 (green) detection.

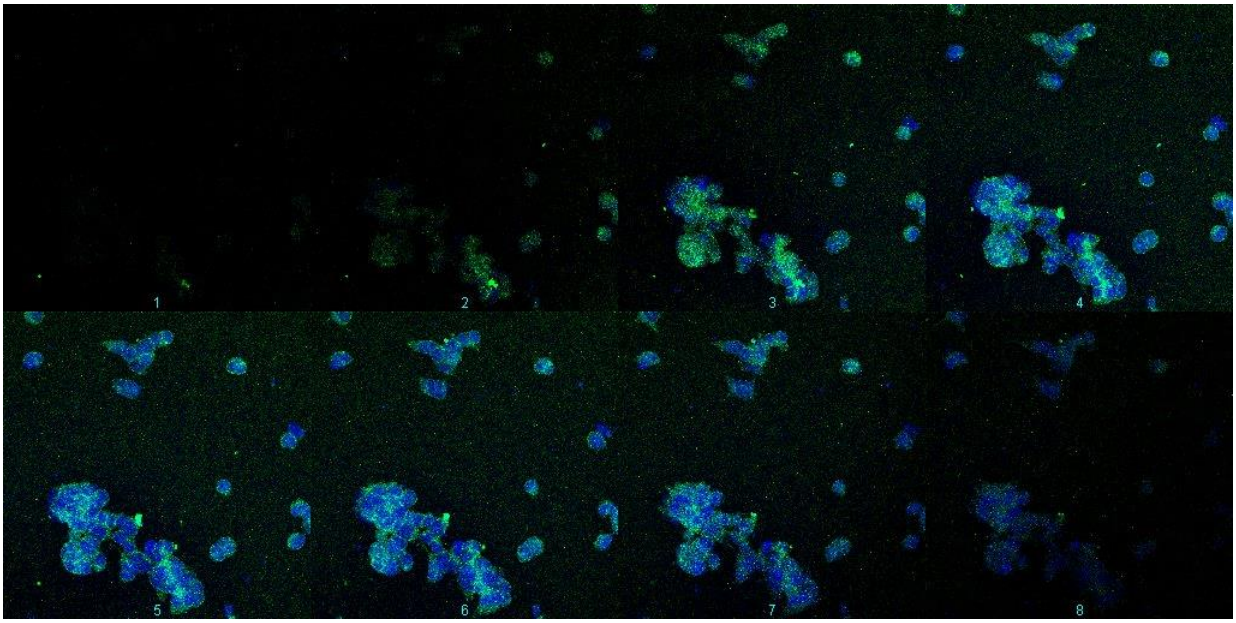


**Figure 8.17- 40x z-stack projections from the Image 2 of 2-hour treatment with Lyso-Gb3**. 9 different projections. PI and Gb3 channel fusion for nuclei (blue) and Gb3 (green) detection.

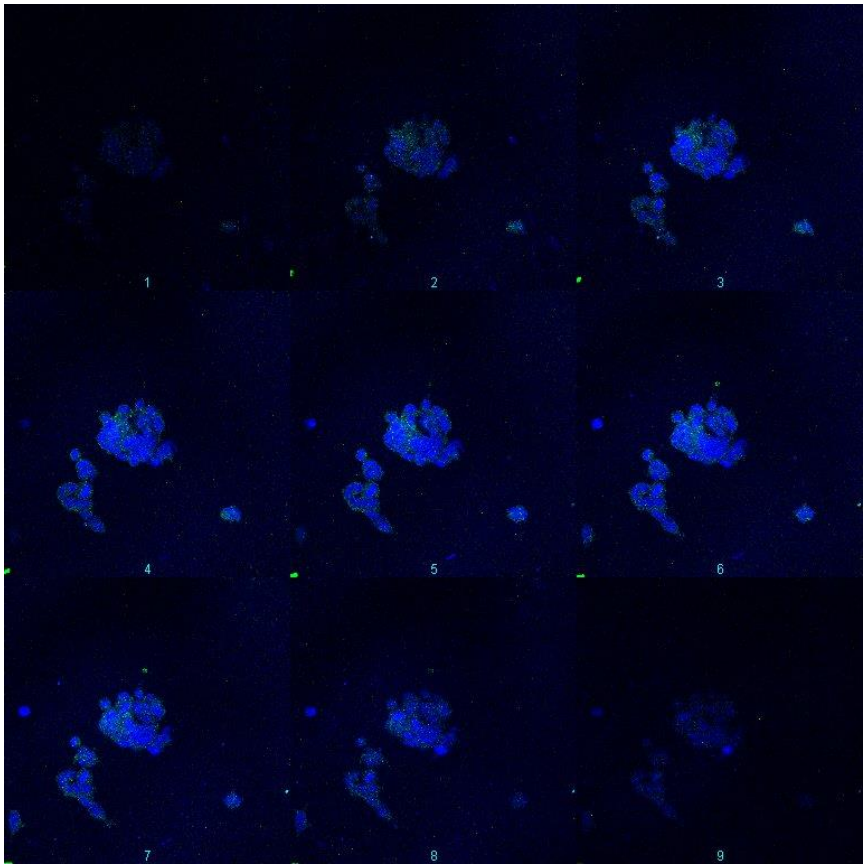


**Figure 8.18 - 40x z-stack projections from the Image 3 of 2-hour treatment with Lyso-Gb3.** 9 different projections. PI and Gb3 channel fusion for nuclei (blue) and Gb3 (green) detection.

**Annex II-** Comparison between Lyso-Gb3 30-minute treatment and the control to this treatment

The graph in Figure 8.19 represents the differences between the three different images obtained from the Lyso-Gb3 treatment with the respective controls.

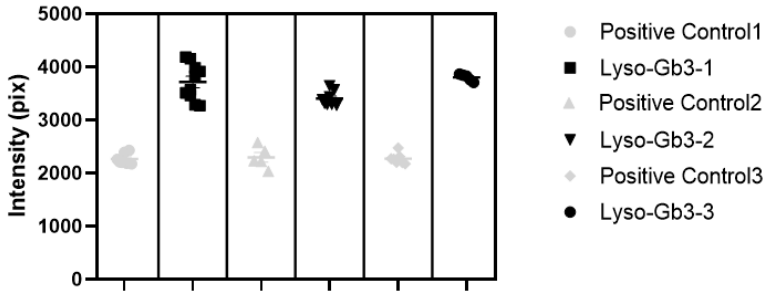


**Figure 8.19 - Incorporation of Lyso-Gb3 for the 30-minute treatment**. Comparison between the three different images obtained for Lyso-Gb3 treatment and the respective controls.

**Annex III-** Comparison of 2 hour-treatment with Lyso-Gb3 or DGJ with controls

The graphs shown in Figures 8.20-8.23 and 8.24-8.27 are for each of the images obtained from the treatment with DGJ or Lyso-Gb3, respectively, and compare with the control.

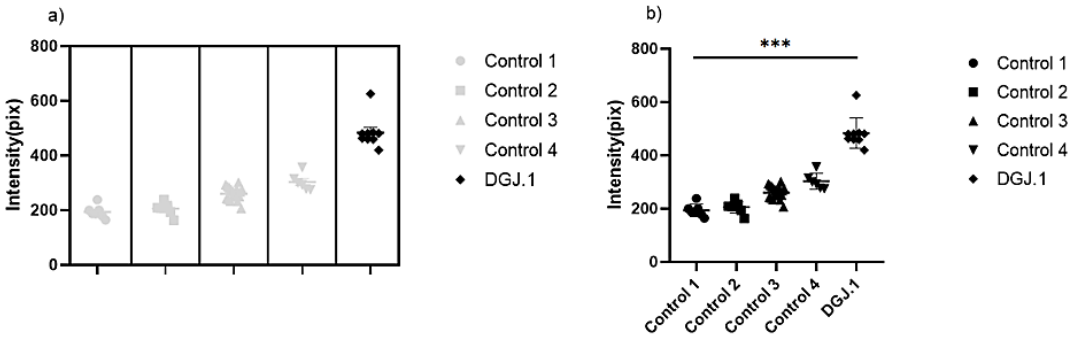


**Figure 8.20 - Gb3 incorporation for the Image 1 of the two-hour DGJ treatment.** a) Comparison of the intensity levels measured in pixels between the 4 controls and the Image 1 obtained from the DGJ treatment for 2 hours. b) Quantification of the intensity levels of all samples. Data are presented as the mean ± SEM. ***p 0.0001 to 0.001 by unpaired *t test.*

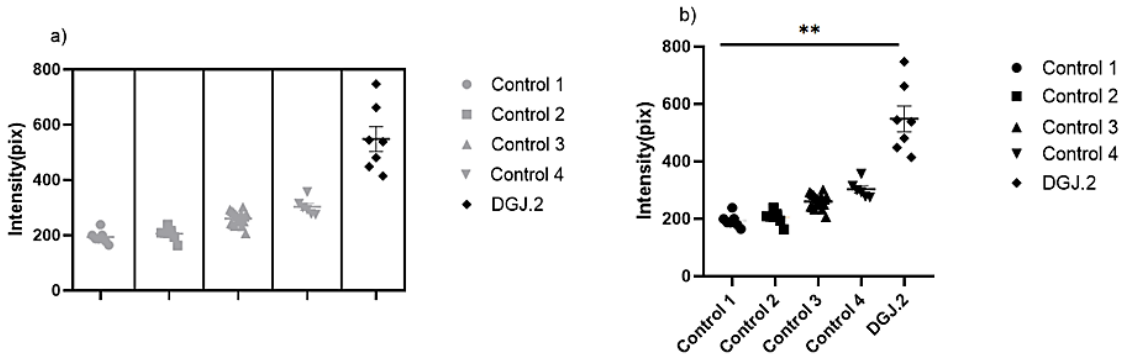


**Figure 8.21 - Gb3 incorporation for the Image 2 of the two-hour DGJ treatment** a) Comparison of the intensity levels measured in pixels between the 4 controls and the Image 2 obtained from the DGJ treatment for 2 hours. b) Quantification of the intensity levels of all samples. Data are presented as the mean ± SEM. **p 0.001 to 0.01 by unpaired *t test*.

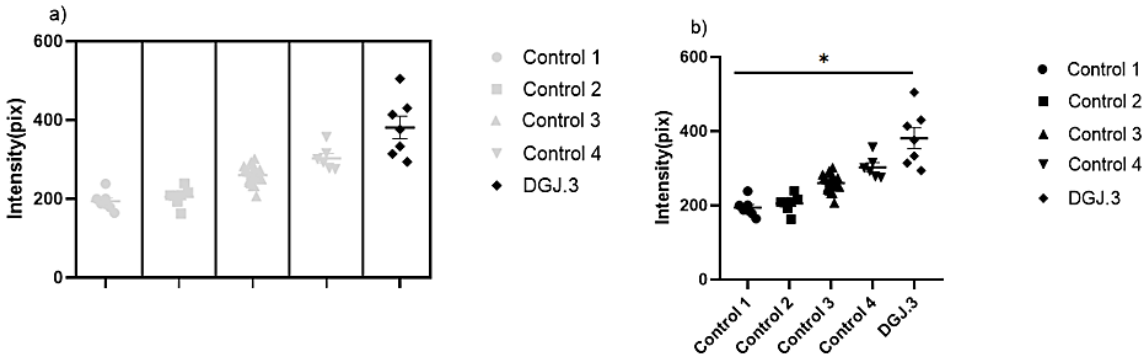


**Figure 8.22 - Gb3 incorporation for the Image 3 of the two-hour DGJ treatment** a) Comparison of the intensity levels measured in pixels between the 4 controls and the Image 3 obtained from the DGJ treatment for 2 hours. b) Quantification of the intensity levels of all samples. Data are presented as the mean ± SEM. *p 0.01 to 0.05 by unpaired *t test.*

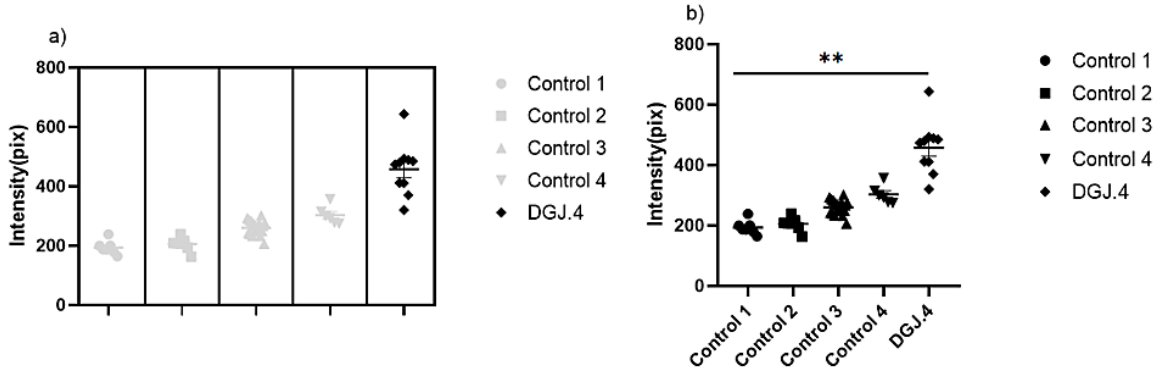


**Figure 8.23 - Gb3 incorporation for the Image 4 of the two-hour DGJ treatment.** a) Comparison of the intensity levels measured in pixels between the 4 controls and the Image 4 obtained from the DGJ treatment for 2 hours. b) Quantification of the intensity levels of all samples. Data are presented as the mean ± SEM. **p 0.001 to 0.01 by unpaired *t test*.

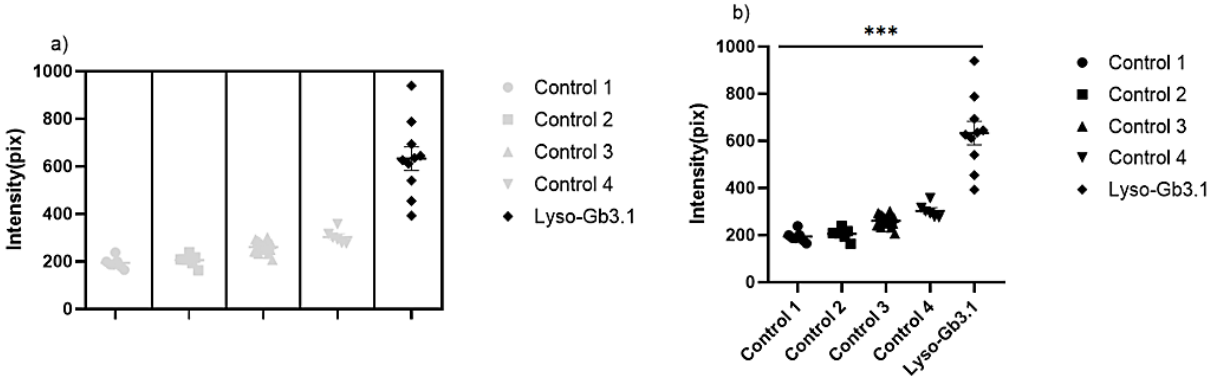


**Figure 8.24 – Lyso-Gb3 incorporation for the Image 1 of the two-hour Lyso-Gb3 treatment.** a) Comparison of the intensity levels measured in pixels between the 4 controls and the Image 1 obtained from the Lyso-Gb3 treatment for 2 hours. b) Quantification of the intensity levels of all samples. Data are presented as the mean ± SEM. ***p 0.0001 to 0.001 by unpaired *t test*.

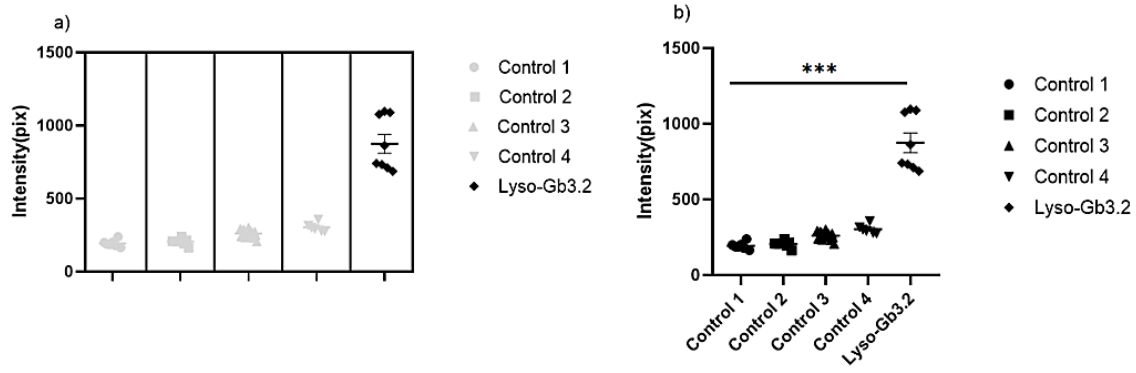


**Figure 8.25 - Lyso-Gb3 incorporation for the Image 2 of the two-hour Lyso-Gb3 treatment.** a) Comparison of the intensity levels measured in pixels between the 4 controls and the Image 2 obtained from the Lyso-Gb3 treatment for 2 hours. b) Quantification of the intensity levels of all samples. Data are presented as the mean ± SEM. ***p 0.0001 to 0.001 by unpaired *t test*.

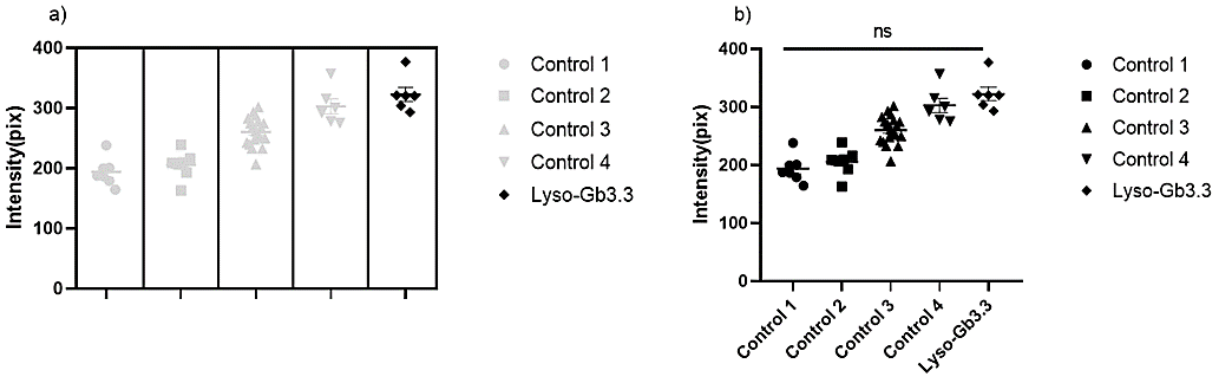


**Figure 8.26 - Lyso-Gb3 incorporation for the Image 3 of the two-hour Lyso-Gb3 treatment.** a) Comparison of the intensity levels measured in pixels between the 4 controls and the Image 3 obtained from the Lyso-Gb3 treatment for 2 hours. b) Quantification of the intensity levels of all samples. Data are presented as the mean ± SEM. *ns* by unpaired *t test*.

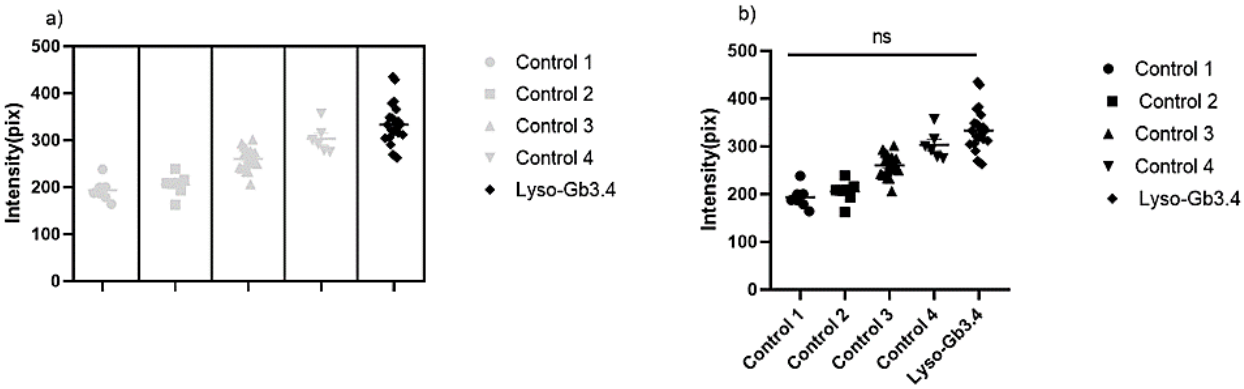


**Figure 8.27 - Lyso-Gb3 incorporation for the Image 4 of the two-hour Lyso-Gb3 treatment.** a) Comparison of the intensity levels measured in pixels between the 4 controls and the Image 4 obtained from the Lyso-Gb3 treatment for 2 hours. b) Quantification of the intensity levels of all samples. Data are presented as the mean ± SEM. ****p < 0.0001 and *ns* by unpaired *t test*.

## **Annex IV-** Comparison of treatment with DGJ and Lyso-Gb3

The individual comparison between each Lyso-Gb3 and DGJ treatment is shown in graphs a), b), c) and d) of Figure 8.28.

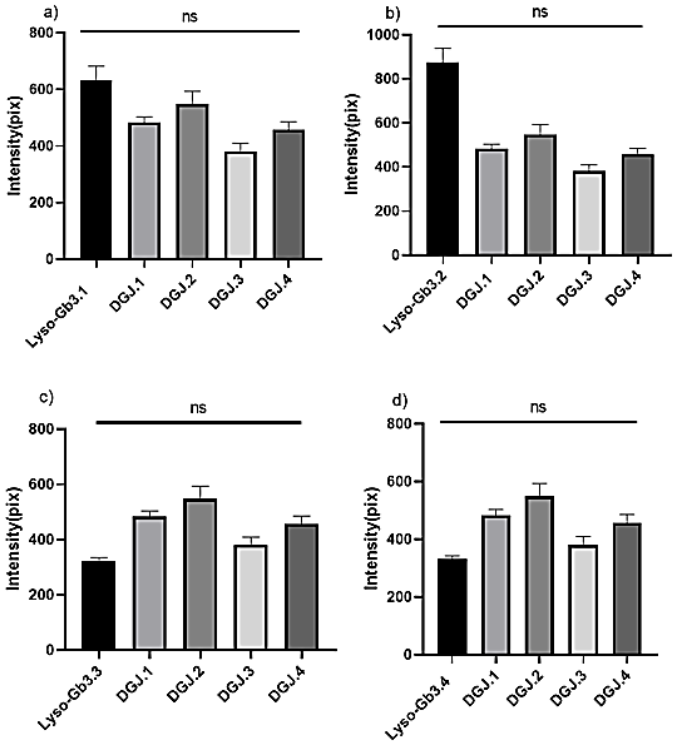


**Figure 8.28 - Comparison between the two-hour treatments**. a) Difference between Lyso-Gb3.1 and the four DGJ treatments b) Difference between Lyso-Gb3.2 and the four DGJ treatments c) Difference between Lyso-Gb3.3 and the four DGJ treatments and d) Difference between Lyso-Gb3.4 and the four DGJ treatments. Data are presented as the mean ± SEM. *ns* by unpaired *t test*.

## **Annex V** - Determining the best dilution for Taq Polymerase for the PCR technique

Three different dilutions (1:20, 1:30 and 1:40) from the available Taq (Taq-mother from the IFIBYNE Institute) were tested to identify which one exhibited the best activity and therefore the ideal one to proceed with the technique. Figure 8.29 shows the bands obtained for the 3 dilutions performed.

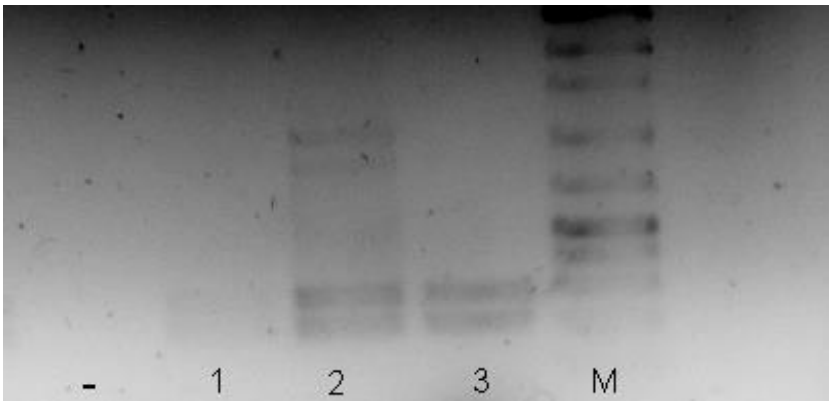


**Figure 8.29 -** Gel obtained by electrophoresis with the bands corresponding to the dilutions performed: (1) 1:20 dilution, (2) 1:40 dilution and (3) 1:30 dilution. M corresponds to the electrophoresis DNA-marker.

By the analysis of Figure 8.29, the dilution nº3 (1:30 of Taq mother) is the one that presents a clearer intensity and without contaminations, therefore it was chosen to perform the technique.

## **Annex VI** – Recipe for TAE 1X

To proceed with the gel electrophoresis run it was necessary to prepare the buffer used, TAE 1X.

Table 8.1 shows the reagents and quantities required for the preparation of TAE 50X, which was further diluted to obtain TAE 1X.

**Table 8.1** - Reagents and respective quantities for the preparation of TAE 50X.

| Reagent | Amount |
|---|---|
| Tris | 242 g |
| EDTA 0.5M | 100 µL |
| Acetic Acid | 57.1 mL |

## **Annex VII** - Classification of samples used in PCR

**Table 8.2** - Classification of the samples used for PCR according to their type and sex. Amount of DNA from each of these samples present in 1µL.

| Number | Sex | Type | Amount of DNA (µg/µL) |
|---|---|---|---|
| 86 | Female | WT | 0,0984 |
| 87 | Female | WT | 0,0991 |
| 88 | Female | WT | 0,1838 |
| 89 | Male | WT | 0,1264 |
| 90 | Male | WT | 0,0348 |
| 91 | Female | WT | 0,1038 |
| 92 | Female | WT | 0,1509 |
| 93 | Male | WT | 0,1500 |
| 94 | Female | WT | 0,1007 |
| 164 | Male | *Gla*-KO | 0,0943 |
| 166 | Male | *Gla*-KO | 0,0726 |
| 167 | Male | *Gla*-KO | 0,0090 |
| 168 | Female | *Gla*-KO | 0,0732 |
| 169 | Female | *Gla*-KO | 0,1252 |
| 170 | Female | *Gla*-KO | 0,0962 |
| 171 | Male | *Gla*-KO | 0,0955 |
| 172 | Male | *Gla*-KO | 0,0818 |
| 173 | Male | *Gla*-KO | 0,1555 |
| 175 | Female | *Gla*-KO | 0,0717 |
| 176 | Female | *Gla*-KO | 0,2020 |